ABSTRACT

WAGNER, BRIAN PAUL. Conventional and Pendeo-epitaxial Growth of Non-Polar GaN$(11\bar{2}0)$ Thin Films on AlN/4H-SiC$(11\bar{2}0)$ Substrates and their Characterization and Reduction in Defect Density. (Under the direction of Dr. Robert F. Davis.)

Non-polar GaN$(11\bar{2}0)$ thin films were deposited on AlN/4H-SiC$(11\bar{2}0)$ substrates via metalorganic vapor phase epitaxy. Atomic force microscopy images revealed that the microstructure of the AlN buffer layer and the subsequently deposited GaN contained a highly oriented growth structure where parallel growth features were aligned in the $[1\bar{1}00]$ direction. Scanning electron microscopy showed that the interfaces between the substrate, buffer layer, and epi-layer were continuous. Cracking was observed in GaN films having a thickness greater than 800 nm. Plan-view transmission electron microscopy analysis revealed stacking faults and threading dislocations with densities of $\sim 1.6 \times 10^{6} cm^{-1}$ and $\sim 3.3 \times 10^{10} cm^{-1}$, respectively. X-ray diffraction confirmed that the GaN was deposited epitaxially in the same orientation as the substrate. The average on- and off-axis x-ray full-width half-maxima of the $(11\bar{2}0)$ and the $(10\bar{1}0)$ reflections were 948 arcsec and 5448 arcsec, respectively.

Coalesced, non-polar GaN$(11\bar{2}0)$ films having volumes of material with reduced densities of dislocations and stacking faults has been achieved from etched stripes via the statistical and experimental determination of the effect of temperature and V/III ratio on the lateral and vertical growth rates of the GaN{0001} faces combined with pendeo-epitaxy. AFM of the uncoalesced GaN(0001) and GaN$(000\bar{1})$

faces revealed growth steps with some steps terminating at dislocations on the former and a pitted surface without growth steps, indicative of decomposition, on the latter. Coalescence was achieved via (a) a two-step route and the parameters of (1) T=1100ºC and V/III=1323 for 1.5hrs and (2) 1020ºC and V/III= 1323 for 1.5hrs and (b) a one-step route that employed T = 1020°C and a V/III ratio = 660 for six hours. The densities of dislocations in the GaN grown vertically over and laterally from the $(11\bar{2}0)$ stripes were ~$4x10^{10}$ cm^{-2} and ~$2x10^{8}$ cm^{-2}, respectively; the densities of stacking fault in these volumes were ~$1x10^{6}$ cm^{-1} and ~$2x10^{4}cm^{-1}$, respectively. Plan view AFM also revealed different microstructures and a reduction in the RMS roughness values from 1.2nm to 0.95nm in these respective regions.

Conventional and Pendeo-epitaxial Growth of Non-Polar GaN $(11\bar{2}0)$ Thin Films on AlN/4H-SiC $(11\bar{2}0)$ Substrates and their Characterization and Reduction in Defect Density

By

Brian Paul Wagner

A thesis submitted to the Graduate Faculty of North Carolina State University in partial fulfillment of the requirements for the Degree of Master of Science

Materials Science and Engineering

Raleigh, NC

April 11th, 2005

APPROVED BY:

_____	_____
Dr. John Mackenzie	Dr. Mark Johnson

_____

Chair of Advisory Committee
Dr. Robert F. Davis

Biography

Brian Paul Wagner was born to Paul and Dorinda Wagner on October 30th, 1978 in Peoria, Illinois. While he was still young, his family moved to the warmer climes of Raleigh, NC, a place to which he would eventually return. Shortly thereafter, his family settled down in a small town named Tega Cay, SC. He spent the next thirteen years living a normal childhood, full of soccer matches, growing pains, and great memories. After graduation from Fort Mill High School in 1997, Brian moved on to Clemson University where he excelled. In May 2002, he graduated Summa Cum Laude with a BS in Ceramic Engineering, first in his class. After deciding to continue his academic career, he attended North Carolina State University under the direction of Dr. Robert F. Davis. The subsequent research is presented here.

Acknowledgements

I would first like to thank Dr. Davis for his guidance and support with my academic life and life beyond the laboratory. I am thankful to have worked under not only a world-class researcher, but an honest, good person. I would also like to thank my committee members, Dr. Johnson and Dr. Mackenzie, for their guidance and for supporting me on this very important endeavor. No thanks would be complete with out thanking Jan Jackson and Edna Deas, the glue that kept me together and everything running smoothly. Further, I would like to thank the members of my research group for their insight and friendship including Zach Reitmeier, Ji-Soo Park, Seann Bishop, Jon Pierce, Bunmi Adekore, Will Mecouch, Ed Preble, and Sharon Kiesel. I'd also like to thank Dr. Dale Batchelor and the entire staff of the AIF, Dr. Dmitri Zakharov and Dr. Zusanna Lilliental-Weber at Lawrence Berkeley National Lab, and Dr. Brian Skromme at Arizona State University. Most importantly, I thank my Mom and Dad. Their love, support, and encouragement has been so important to me, more than they will ever know. Thank you Mom and Dad.

Table of Contents

Item	Page
List of Tables …….	vi
List of Figures ……	vii
1. Introduction ……..	1
References …….	5
2. Growth and Characterization of Epitaxial GaN Thin Films on 4H-SiC $(11\bar{2}0)$ Substrates ……	8
2.1 Abstract ……..	9
2.2 Introduction ……...	9
2.3 Experimental Details ……	10
2.4 Results and Discussion …….	11
2.5 Summary ……	14
2.6 Acknowledgements ……..	14
2.7 Addendum …….	15
2.8 References …….	16
2.9 Tables …….	17
2.10 Figures ……	18
3. Growth and Characterization of Pendeo-epitaxial GaN $(11\bar{2}0)$ on 4H-SiC $(11\bar{2}0)$ Substrates……	20
3.1 Abstract ……	21
3.2 Introduction …….	22
3.3 Experimental Procedure …….	24
3.4 Results and Discussion ……	26
3.5 Conclusions ……..	35
3.6 References ……	37
3.7 Tables ……	40
3.8 Figures ……..	41
4. Future Work ……	50
Appendices ……..	52
5. Appendix I: Chapter 2 Addendum ……	53
5.1 Experimental Procedure ……	53
5.2 Results and Discussion ……..	54
5.3 Tables ……	58
5.4 Figures ……..	59

6. Appendix II: Clean-room Processes for the Production of Pendeo-epitaxial Seed Posts…… 67
6.1 Cleaning the GaN Wafers ……. 67
6.2 AZ5214E Photoresist Coating ……... 67
6.3 Alignment and Exposure …… 67
6.4 Develop ……. 68
6.5 Ni Deposition ……. 68
6.6 Lift-off …… 69
6.7 Pendeo-epitaxy Clean-room Process Chemical Details …… 70

List of Tables

Page

Chapter 2

1. Values of the $(11\bar{2}0)$ and (0001) lattice constants and the coefficients of thermal expansion in the [0001] direction for GaN, AlN and 4H-SiC single crystals …….. 17

Chapter 3

1. Results of DOE studies with n=2 full factorial with a center-point to determine the effect of temperature and V/III ratio on the growth rate of GaN vertically from the $(11\bar{2}0)$ surface (V) and laterally from both the Ga-terminated (0001) face (Lg) and the N-terminated $(000\bar{1})$ face (Ln) and on the ratios Rg (Lg/V) and Rn (Ln/V) ……. 40

Appendix I

1. Depth profile C-V results acquired at 1MHz on $[11\bar{2}0]$- and [0001]-oriented GaN thin films …….. 58

List of Figures

Page

Chapter 2

1. Atomic force microscopy images of (a) a typical 100 nm AlN buffer layer, and (b) and (c) epitaxial GaN films subsequently grown on the AlN …… 18

2. Cross-sectional SEM image of a cracked 1 μm thick epitaxial GaN $(11\bar{2}0)$ film grown on an AlN/4H-SiC $(11\bar{2}0)$ substrate …… 18

3. Cross-sectional TEM image of a GaN $(11\bar{2}0)$ film with a thickness of 1μm grown on an 0.1 μm thick AlN buffer layer deposited on a 4H-SiC $(11\bar{2}0)$ substrate …….. 19

Chapter 3

1. SEM micrographs showing (a) the cross section and (b) the top and sidewall of a representative GaN stripe, produced via ICP etching, and used as a template for pendeo-epitaxial re-growth of a GaN film …….. 41

2. SEM micrographs (15,000x) of uncoalesced pendeo-epitaxial samples that exhibit the growth characteristics and features resulting from the use of growth parameters involving (a) low temperature (1020ºC) and an intermediate V/III ratio (1323) for 40 mins. and (b) high temperature (1100°C) and an intermediate V/III ratio (1323) for 40 mins. ……. 42

3. TEM micrographs acquired from an uncoalesced sample grown at 1020°C using a V/III ratio = 1323 for 40 mins. g = [0002] and $[1\bar{1}00]$ in (a) and (b), respectively. …….. 43

4. AFM micrograph showing growth steps on the (0001) sidewall of an uncoalesced GaN film grown under the same conditions as the material used to produce Figure 3 …… 44

5. AFM micrograph of an uncoalesced GaN$(000\bar{1})$ sidewall after heating under for 40 mins. under the conditions of T = 1020°C and V/III ratio = 1323 …… 45

6. (a) Cross-sectional and (b) plan view SEM micrographs showing coalesced pendeo-epitaxial GaN achieved using a two-step process route …… 46

7. (a) Cross-sectional and (b) plan view SEM micrographs showing coalesced pendeo GaN achieved using the growth conditions of T = 1020ºC and V/III ratio = 660 for six hours ... 47

8. Cross-sectional and (b) plan view TEM micrographs of the Coalesced pendeo-epitaxial sample shown in Figure 7 was Acquired …… 48

9. AFM micrographs of the surface of the coalesced Pendeo -epitaxial GaN films grown at T = 1020ºC and V/III= 660 ….. 49

Appendix I

1. Graph used to predict Silane flow (μmol/min) needed to achieve the desired number of carriers in GaN(0001) thin films 59

2. Atomic % Si incorporated during growth into $[11\bar{2}0]$- and [0001]-oriented GaN thin films …… 60

3. SIMS results of atomic concentrations of H, C, and O as a function of depth in Si-doped $[11\bar{2}0]$-and [0001]-oriented GaN thin films …….. 61

4. SIMS results of atomic concentrations of H, C, and O as a function of depth in undoped $[11\bar{2}0]$-and [0001]-oriented GaN thin films …….. 62

5. PL spectra of undoped and doped GaN(0001) ……. 63

6. PL spectra of undoped and doped GaN$(11\bar{2}0)$ ……. 64

7. PL spectra of undoped GaN$(11\bar{2}0)$ and GaN(0001) …… 65

8. PL spectra of Si-doped GaN$(11\bar{2}0)$ and GaN(0001) ……... 66

I. Introduction

The Group III-nitrides have become important materials for short-wavelength photonic and high-frequency devices and applications [1]. At present, the majority of the III-nitride films and device structures are grown on the (0001) plane of sapphire and SiC [2]. Gallium nitride and its alloys normally possess the wurtzite structure. The ionic contribution to the bonding in this structure gives rise to macroscopic spontaneous polarization along the <0001> polar axes. The total polarization of [0001]-oriented nitride heterostructures, e.g., AlGaN/GaN device layers, has both spontaneous and piezoelectric components [3,4]. These components produce fixed charges of opposite sign at the {0001} surfaces that change abruptly at every surface or hetero-interface. These polarization-induced fields have been employed for the creation of a two-dimensional electron gas in high electron mobility transistors (HEMT) [5,6]. These fields also induce electrostatic fields parallel to the c-axis [7] that spatially separate electrons and holes within quantum well structures (the quantum-confined Stark effect). This spatial separation causes a reduction in oscillator strength and a red shift in optical transitions due to a reduction in the quantum recombination efficiency [8] in quantum wells in III-nitride optoelectronic devices grown along the polar c-axis. To circumvent these effects, non-polar GaN-based layers have been grown and characterized on non-polar substrates including a-plane 4H-SiC $(11\bar{2}0)$ [9], r-plane sapphire $(1\bar{1}02)$ [10,11], a-plane sapphire $(11\bar{2}0)$ [12], and tetragonal (γ) $LiAlO_2$ [13]. Devices have been fabricated [14-18] on non-polar GaN-based layers, and direct comparisons of non-polar and polar devices have also been reported [19].

Non-polar GaN-based layers and device structures, though free of electrostatic fields, continue to be grown at this writing on the foreign substrates previously noted and contain domains, similar densities of dislocations and stacking faults in the manner of the materials grown along [0001] [20]. Dislocations in GaN (1) have energy levels in the band gap that allow carrier recombination from donor states and states at the bottom of the conduction band, (2) act as conduits for charge transport that result in high leakage currents and slow breakdown of rectifying contacts, and (3) reduce significantly the lifetime of laser diodes [1,2,21]. Several research groups have determined that lateral epitaxial overgrowth (LEO) and pendeo-epitaxy (PE) can significantly reduce the dislocation density in GaN and AlGaN films grown on sapphire(0001) [22-26] and SiC(0001) [27-35]. Further, LEO [36-38] and selective area lateral epitaxy [39] on r-plane sapphire $(1\bar{1}02)$ have been used to produce non-polar GaN-based films that posses significantly reduced densities of dislocation and stacking faults as well as surface microstructures free of pits and other defects derived from anisotropic growth in the $(11\bar{2}0)$ plane [40,41].

The objectives of the research reported herein have been (1) the conventional and pendeo-epitaxial growth of non-polar of GaN $(11\bar{2}0)$ films on 4H-SiC $(11\bar{2}0)$ substrates and (2) the structural, morphological, microstructural, optical, electrical and chemical characterization of the final growth surface and the interior of the bulk films with an emphasis on the determination of the types, densities and distributions of the line and planar defects in the materials.

Chapter 2 describes the metalorganic vapor phase epitaxial growth and characterization of non-polar GaN $(11\bar{2}0)$ films on 4H-SiC $(11\bar{2}0)$ substrates where no growth techniques were employed to reduce the densities of dislocations and stacking faults. The use of and the results from atomic force microscopy (AFM), scanning electron microscopy (SEM), transmission electron microscopy (TEM), and X-ray diffraction (XRD) studies to determine the orientation of the as-grown microstructure, the nature and density of the line and planar defects and the orientation of the films are detailed.

Chapter 3 details the achievement of the reduction in densities of stacking faults and threading dislocations in non-polar GaN $(11\bar{2}0)$ films on AlN/4H-SiC $(11\bar{2}0)$ substrates via pendeo-epitaxy (PE). SEM, AFM and TEM revealed that coalescence between laterally growing <0001>-oriented wings from previously etched $(11\bar{2}0)$ stripes was accomplished via both a two-step and an one-step route. TEM further revealed that the densities of dislocations in the GaN grown vertically over and laterally from the $(11\bar{2}0)$ stripes were ~4×10^{10} cm^{-2} and ~2×10^{8} cm^{-2}, respectively; the densities of stacking fault in these volumes were ~1×10^{6} cm^{-1} and ~$2\times10^{4} cm^{-1}$, respectively.

Appendix 1 summarizes an investigation into the differences of Si-doped GaN on AlN/4H-SiC $(11\bar{2}0)$ and AlN/6H-SiC(0001) substrates. Photoluminescence spectroscopy, capacitance-voltage measurements, secondary ion mass spectrometry, and Hall measurements were employed to discern the differences and the similarities between the GaN films grown on these two substrates.

Appendix 2 details the steps in the production of the GaN seed posts (etched stripes) used for PE. Included are the details of the cleanroom process and the subsequent use of the inductively coupled plasma etching system used to produce the previously mentioned GaN stripes.

1.2 References

[1] S.J. Pearton, J.C. Zolper, R.J. Shul, F. Ren, *J. Appl. Phys.* **86** (1999) 1.

[2] S.C. Jain, M. Willander, J. Narayan, R. Van Overstraeten, *J. Appl. Phys.* **87** (2000) 965.

[3] F. Bernardini, V. Fiorentini, *Phys. Rev. B* **56** (1997) R10024.

[4] F. Bernardini, V. Fiorentini, *Phys. Rev. B* **57** (1998) R9427.

[5] I.P. Smorchkova, C.R. Elsass, J.P. Ibbetson, R. Vetury, B. Heying, P. Fini, E. Haus, S.P. DenBaars, J.S. Speck, U.K. Mishra, *J. Appl. Phys*. **86** (1999) 4520.

[6] O. Ambacher et al, *J. Appl. Phys.* **85** (1999) 3222.

[7] T. Takeuchi, S. Sota, M. Katsurgawa, M. Komori, H Takeuchi, H. Amano, I. Akasaki, *Jpn. J. Appl. Phys.* Part 2 **36** (1997) L382.

[8] J.S. Im, H. Kollmer, J. Off, A. Sohmer, F. Scholz, A. Hangleiter, *Phys. Rev. B* **57** (1998) R9435.

[9] B.P. Wagner, E.A. Preble, Z.J. Reitmeier, R.F. Davis, D.N. Zakharov, Z. Liliental-Weber, *Mat. Res. Soc. Symp. Proc.* **798** (2004) Y10.34.1.

[10] M.D. Craven, S.H. Lim, F. Wu, J.S. Speck, S.P. DenBaars, *Appl. Phys. Lett.* **81** (2002) 469.

[11] B.A. Haskell, F. Wu, S. Matsuda, M.D. Craven, P.T. Fini, S.P. DenBaars, J.S. Speck, S. Nakamura, *Appl. Phys. Lett.* **83** (2003) 1554.

[12] Sugianto, R.A. Sani, P. Arifin, M. Budiman, M. Barwami, *J. Crystal Growth* **221** (2000) 311.

[13] P. Waleriet, O. Brandt, A. Trampert, H.T. Grahn, J. Menninger, M. Rammsteiner, M. Reiche, K.H. Ploog, *Nature* **406** (2000) 865.

[14] C. Chen, V. Adivarahan, J. Yang, M. Shatalov, E. Kuoksis, M.A. Khan, *Jpn. J. Appl. Phys.* **42** (2003) L1039.

[15] V. Adivarahan, C. Chen, J. Yang, M. Gaveski, M. Shatalov, G. Simin, M.A. Khan, *Jpn. J. Appl. Phys.* **42** (2003) L1136.

[16] W.H. Sun et al., *Appl. Phys. Lett.* **83** (2003) 2599.

[17] H.M. Ng, A. Bell, F.A. Ponce, S.N.G. Chu, *Appl. Phys. Lett.* **83** (2003) 653.

[18] S. Iyer, D.J. Smith, A. Bhattacharyya, K. Ludwig Jr., T.D. Moustakas, *Mat. Res. Soc. Symp. Proc.* **743** (2003) L3.20.1.

[19] E. Kuokstis et al., *Appl. Phys. Lett.* **81** (2002) 4130.

[20] D.N. Zakharov, Z. Liliental-Weber, B.P. Wagner, Z.J. Reitmeier, E.A. Preble, R.F. Davis, *Mat. Res. Soc. Symp. Proc.* **798** (2004) Y5.28.1.

[21] S.Nakamura, M. Senoh, S.I. Nagahama, T. Matushita, K. Kiyoku, Y. Sugimoto, T. Kozaki, H. Umemoto, M. Sano, T. Mukai, *Jpn. J. Appl. Phys*., Part 2 **38** (1999) L226.

[22] D. Kapolnek, S. Keller, R. Vetury, R.D. Underwood, P. Kozodoy, S.P. DenBaars, U. K. Mishra, *Appl. Phys. Lett.* **71** (1997) 1204.

[23] H. Marchand, J.P. Ibbetson, P.T. Fini, S. Chichibu, S.J. Rosner, S. Keller, S.P. DenBaars, J.S. Speck, U. K. Mishra, in *25th Int. Symp. Compound. Semiconductors.* IOP Publishing, Nara, Japan, 1998, p. 681.

[24] H. Kim, C. Sone, O.H. Nam, Y.J. Park, T. Kim, *Appl. Phys. Lett.* **75** (1999) 4109.

[25] Sakai, H. Sunakawa, A. Kimura, A. Usui, *Appl. Phys. Lett.* **76** (2000) 442.

[26] X. Zhang, P.D. Dapkus, and D. H. Rich, *Appl. Phys. Lett.* **77** (2000) 1496.

[27] A.M. Roskowski, E.A. Preble, S. Einfeldt, P.M. Miraglia, J. Schuck, R. Grober, R.F. Davis, *Opto-electronics Review* **10** (2002) 261.

[28] O. H. Nam, M.D. Bremser, T.S. Zheleva, R. F. Davis, *Appl. Phys. Lett.* **71** (1997) 2638.

[29] O. H. Nam, T. S. Zheleva, M.D. Bremser, R. F. Davis, *J. Elect. Mater.* **27** (1998) 233.

[30] R. F. Davis, T. Gehrke, K.J. Linthicum, T.S. Zheleva, E.A. Preble, P. Rajagopal, C.A. Zorman, M. Mehregany, *J. Cryst. Growth* **225** (2001) 134.

[31] R. S. Q. Fareed, J. W. Yang, J. Zhang, V. Adivarahan, V. Chaturvedi, M. A. Khan, *Appl. Phys. Lett.* **77** (2000) 2343.

[32] T. Gehrke, K.J. Linthicum, E. Preble, P. Rajagopal, C. Ronning, C. Zorman, M. Mehregany, R. F. Davis, *J. Electron. Mater.* **29** (2000) 306.

[33] K. Linthicum, T. Gehrke, D. Thomson, E. Carlson, P. Rajagopal, T. Smith, D. Batchelor, R. F. Davis, *Appl. Phys. Lett.* **75,** (1999) 196.

[34] D. B. Thomson, T. Gehrke, K.J. Linthicum, P. Rajagopal, R. F. Davis, *MRS Internet J. Nitride Semicond. Res.* **4S1** (1999) G3.37.

[35] T. Zheleva, S. Smith, D. Thomson, K. Linthicum, *J. Electron. Mater.* **28** (1999) L5-L8.

[36] M.D. Craven, S.H. Lim, F. Wu, J.S. Speck, S.P. DenBaars, *Appl. Phys. Lett.* **81** (2002) 1201.

[37] B.A. Haskell, F. Wu, M.D. Craven, S. Matsuda, P.T. Fini, T. Fujii, K. Fujito, S.P. DenBaars, J.S.Speck, S. Nakamura, *Appl. Phys. Lett.* **83** (2003) 644.

[38] C. Chen, J. Yang, H. Wang, J. Zhang, V. Adivarahan, M. Gaveski, E. Kuokstis, Z. Gong, M. Su, M.A. Khan, *Jpn. J. Appl. Phys.* **42** (2003) L640.

[39] C. Chen et al., *Jpn. J. Appl. Phys.* **42** (2003) L818.

[40] D.S. Li, H. Chen, H.B. Yu, X.H. Zheng, Q.Huang, J.M. Zhou, *J. Crystal Growth* **265** (2004) 107.

[41] H. Wang, C. Chen, J. Zhang, M. Gaevski, M. Su, J. Yang, M.A. Khan, *Appl. Phys. Lett.* **84** (2004) 499.

2. Growth and Characterization of Epitaxial GaN Thin Films on 4H-SiC $(11\bar{2}0)$ Substrates

Brian P. Wagner[1], E.A. Preble[3], Z.J. Reitmeier[1], R.F. Davis[1], D.N. Zakharov[2], and Z. Liliental-Weber[2],

[1]North Carolina State University, Raleigh, NC 27695, [2]Lawrence Berkeley National Laboratory, MS 62-203, Berkeley, CA 94720, [3]Kyma Technologies, Inc., Raleigh, NC

Published in: Mat. Res. Soc. Symp. Proc. Vol. 798, Y10.34.1

2.1 Abstract

GaN thin films were grown via metalorganic vapor phase epitaxy on a-plane 4H-SiC substrates on which had been deposited an AlN buffer layer. Atomic force microscopy images revealed that the microstructure of the AlN buffer layer and the subsequently deposited GaN had a highly oriented growth structure where parallel growth features propagated in the $[1\bar{1}00]$ direction. Scanning electron microscopy showed that the interfaces between the substrate, buffer layer, and epi-layer were continuous. Cracking was observed in GaN films having a thickness greater than 800 nm. Plan-view transmission electron microscopy analysis revealed stacking faults and threading dislocations with densities of ~$1.6 \times 10^{6} cm^{-1}$ and ~ $3.3 \times 10^{10} cm^{-1}$, respectively. X-ray diffraction confirmed that the GaN was deposited epitaxially in the same orientation as the substrate. The average on- and off-axis x-ray full-width half-maxima of the $(11\bar{2}0)$ and the $(10\bar{1}0)$ reflections were 948 arcsec and 5448 arcsec, respectively.

2.2 Introduction

Group III-nitrides are inherently piezo- and pyroelectric materials due to their wurtzite structure. The polar axis in a wurtzite crystal is aligned along the [0001] direction. The polarization fields of this orientation result in reduced quantum recombination efficiency in quantum well structures, and a red-shift in optical emission wavelengths. Electrostatic fields and piezo- and pyro-electric characteristics are absent along all directions perpendicular to [0001]. The absence of an electric field yields a distinct advantage for high-efficiency GaN-based LEDs and laser diodes compared to conventionally [0001] oriented structures similarly grown on sapphire and SiC.[1-3]

Recently, growth of GaN in non-polar directions has been attempted on tetragonal (γ) $LiAlO_2$ [4], and on $(1\bar{1}02)$ r-plane sapphire.[5] The principal objective of the research reported herein has been the growth via metalorganic vapor phase epitaxy (MOVPE) and characterization of non-polar GaN $(11\bar{2}0)$ on SiC $(11\bar{2}0)$ substrates having an AlN buffer layer.

2.3 Experimental Details

The epitaxial AlN buffer layers and the subsequently deposited epitaxial GaN films were grown in-situ in a cold-wall, vertical, pancake-style metalorganic vapor phase epitaxy (MOVPE) system on research grade, on-axis 4H-SiC(11.0) substrates which had been immersed in a 10% HF solution to remove the native oxide. The AlN buffer layers and the GaN films were grown at 20 Torr and at sample platter temperatures of 1100°C and 1015°C, respectively. The precursor species (mass flow rates) of tri-methylaluminum (TMA; 5.4 μmol/min), tri-ethylgallium (TEG; 101 μmol/min) and ammonia (NH_3; 0.14 mol/min) were mixed with a purified H_2 diluent (3 slm) in a two-inch internal diameter sleeve located two inches above the substrate. X-ray diffraction was conducted using a Phillips X'pert Materials Research Diffractometer (MRD) equipped with a four-fold Ge(220) monochromator and a three-fold Ge(220) analyzer. A copper X-ray source at a power setting of 40kV and 45mA was used to obtain the spectra. The surface morphologies of the AlN and the GaN was determined via atomic force microscopy (AFM) in the tapping mode using a Digital Instruments D3000 AFM with a silicon tip. Images of the surfaces and the sidewalls of the epitaxial GaN films were obtained at 25,000X using a JEOL 6400 FE scanning electron microscope (SEM). Cross-sectional and plan-view samples were prepared for transmission electron microscopy

(TEM) and high resolution electron microscopy (HREM) using the sequence of mechanical polishing, dimpling to a thickness of 10μm and argon ion milling at 5kV until perforation. The TEM and HREM utilized a JEOL 3010 microscope operated at 300kV to acquire the necessary images.

2.4 Results and Discussion

Atomic force microscopy of the AlN buffer layer revealed oriented features parallel to the $[1\bar{1}00]$ direction. Analogous features were also observed in the subsequently deposited GaN epitaxial layers that mimicked the underlying AlN buffer layer. These features are shown in Figures 1 (a) and (b), respectively, and are similar to those observed on the surface of a-plane GaN grown on r-plane sapphire.[5] Figure 1(c) reveals two types of features with one feature parallel to the [0001] direction and the other perpendicular to the $[1\bar{1}00]$ direction and the features shown in figure 1(a) and (b). The features that are visible on the 20μm x 20μm AFM image, (c), are also visible using optical microscopy with 400X magnification. The origin of these latter features has not been determined; however, they are likely caused by the anisotropy in the growth rates along the $[1\bar{1}00]$ and [0001] directions.

Cross-sectional SEM revealed continuous interfaces between the substrate, buffer layer, and epi-layer. No surface features were resolved. Further, the presence of cracks in the epitaxial GaN film were observed by sectioning the sample parallel to the c-axis, or perpendicular to the $[1\bar{1}00]$ direction. Figure 2 shows a characteristic crack in a 1 μm GaN film; all cracks that occurred in these samples were perpendicular to the [0001] direction.

The differences in the (0001) lattice parameters and the coefficients of thermal expansion (CTE) along the [0001] direction given in Table 1 indicate that the epitaxial GaN films should be in tension along the [0001] axis relative to the 4H-SiC $(11\bar{2}0)$ substrate if the latter is assumed to be rigid in relation to the epitaxial GaN film. A definitive explanation for when and why cracking occurs in samples similar to Figure 2 has not been determined; however, it may be related to the tensile stress along the [0001] direction due to a mismatch in thermal expansion coefficients

The elimination of cracking in the GaN films was investigated using two different process routes. The simpler approach was to reduce the thickness of the epitaxial GaN. Crack-free GaN, without strain layer engineering, has been grown to a thickness of 750 nm. The second approach was to insert a 50 nm AlN interlayer when the GaN thickness reached 800 nm. The underlying reasoning was that since the [0001] and $[11\bar{2}0]$ lattice parameters and the CTE along the [0001] in AlN are smaller than the analogous lattice parameters and CTE in GaN, an AlN interlayer would introduce a compressive stress in the subsequently grown films both at the growth temperature and on cooling that would counter the tensile stresses that caused the cracking. The 800nm thick GaN film did not crack; however, a subsequently grown 1μm thick GaN film containing one AlN interlayer and a 1.6 μm thick GaN film containing three evenly spaced AlN interlayers displayed cracking. Thus, the interlayers had little effect on the cracking behavior of the epitaxial GaN films. Further, the total GaN thickness probably has more influence over the onset of cracking in these epitaxial GaN $(11\bar{2}0)$ films on 4H-SiC $(11\bar{2}0)$ substrates.

Transmission electron microscopy of the defect microstructure within the GaN $(11\bar{2}0)$ films revealed both planar and line defects. Contrast attributed to stacking

faults (SF) was observed in bright field images taken in plan-view configuration along the $[1\bar{1}20]$ zone axis. The length of the SF varied from several tens of nanometers to several tens of micrometers. The SF density was measured to be approximately 1.6×10^6 cm^{-1}. The highest contrast from these faults was observed in bright field images taken using a two-beam condition with $g_{11\underline{0}0}$. The SFs were terminated by Shockley partial dislocations. The density of these dislocations, which are out of contrast, was $\sim 1.4 \times 10^{10} cm^{-2}$. Threading dislocations having a density of $\sim 3.3 \times 10^{10} cm^{-2}$ and in strong contrast for the same imaging condition were also observed. The latter could be interpreted as having either pure screw (**b**=1/2*(0001)) or mixed ($b=1/3*(1\bar{1}23)$) character. Related studies of the microstructure in cross-section revealed the origins of the threading dislocations to be at both the AlN buffer layer/SiC interface and the GaN/AlN interface, as shown in figure 3.

X-ray diffraction confirmed that the GaN was deposited epitaxially in the same orientation as the substrate, as revealed by the presence of the $(1\bar{1}20)$ reflections and the absence of the (0002) reflections at $2\theta = 34.604°$. Omega rocking curves were performed on the on-axis $(1\bar{1}20)$ reflections and on the off-axis $(10\bar{1}0)$ reflections to characterize the crystal quality of the a-plane GaN $(1\bar{1}20)$. The average full width at half maximum (FWHM) values for an un-cracked GaN sample with a thickness of 750 nm were 949 arcsec and 5488 arcsec for the on- and off-axis reflections, respectively. Further microstructural analysis is required to correlate the dislocation character with the rocking curve values.

2.5 Summary

Thin films of AlN $(11\bar{2}0)$ and GaN $(11\bar{2}0)$ were grown via metalorganic vapor phase epitaxy on 4H-SiC $(11\bar{2}0)$ substrates. Atomic force microscopy studies revealed aligned growth features perpendicular to the [0001] axis. Scanning electron microscopy images showed that the interfaces between the substrate, buffer layer, and epi-layer were continuous. Cracking was observed in GaN films having a thickness greater than 800 nm. The defect microstructure of the GaN $(11\bar{2}0)$ is dominated by stacking faults terminated by Shockley partial dislocations, and threading dislocations that originate at the AlN buffer layer/SiC substrate interface and the GaN/AlN interface. X-ray diffraction confirmed that the overgrown layers were epitaxial in relation to the 4H-SiC $(11\bar{2}0)$ substrate. Omega rocking curves showed that the average values of the FWHM for an un-cracked GaN film with having a thickness of 750 nm were 949 arcsec and 5,488 arcsec, as determined from on-axis $(11\bar{2}0)$ and off-axis $(10\bar{1}0)$ reflections, respectively.

2.6 Acknowledgements

The research reported herein was sponsored by the Office of Naval Research via the University of California at San Diego under contract N00014-98-1-0654, and monitored by C. Wood. R.F. Davis was supported in part by the Kobe Steel, Ltd. University Professorship. B.P. Wagner was supported in part by a GAANN Fellowship.

2.7 Addendum

Additional research was conducted to compare the silicon doping characteristics of GaN(0001) versus GaN $(11\bar{2}0)$. Discussions of the results acquired from secondary ion mass spectroscopy, depth profile capacitance-voltage, and low temperature photoluminescence of these doped films are presented in Appendix I. The experimental details describing each of the aforementioned measurement/analysis techniques are included.

2.8 References

1. Y.J. Sun, O. Brandt, and K.H. Ploog, Journ. Vac. Sci. and Tech.-B, 4 21 (2003).

2. F. Bernardini and V. Fiorentini, Phys. Rev. B 57, R9427 – R9430 (1998).

3. F. Bernardini and V. Fiorentini, Phys. Rev. B 56, R10024 – R10027 (1997).

4. P. Waleriet, O. Brandt, A. Trampert, H.T. Grahn, J. Menninger, M. Ramsteiner, M. Reiche, and K. H. Ploog, Nature 406, 865 (2000).

5. M.D. Craven, S.H. Lim, F. Wu, J.S. Speck, and S.P. DenBaars, Appl. Phys. Lett. 81, 469 (2002).

6. M. Tanaka, S. Nakahata, K. Sogabe, H. Nakata, M. Tabioka, Jpn. J. Appl. Phys. 36, L1062 (1997).

7. R. Reeber et al, J. Mater. Res. 15, 43 (2000).

8. M. Leszczynski et al, J. Appl. Phys 76, 4909 (1994).

9. Z. Li and R.C. Bradt, J. Amer. Cer. Soc. 70, 445 (1987).

2.9 Tables

Table 1. Values of the $(11\bar{2}0)$ and (0001) lattice constants and the coefficients of thermal expansion in the [0001] direction for GaN, AlN and 4H-SiC single crystals.

Material	**(1120)(Å) @ 300K**	**(0001)(Å) @ 300K**	**Bulk CTE; @ 1000K**
GaN, Bulk[6]	3.189	5.185	4.75 E-6/K[8]
AlN, Bulk[6]	3.111	4.980	2.27 E-6/K[9]
4H-SiC, Bulk[7]	3.073	c/2=5.0265	4.43 E-6/K[10]

2.10 Figures

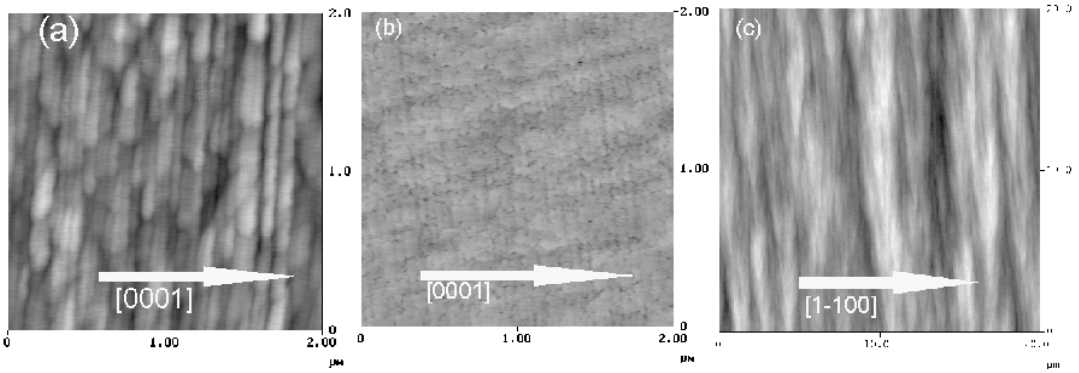

Figure 1. Atomic force microscopy images of (a) a typical100 nm AlN buffer layer, and (b) and (c) epitaxial GaN films subsequently grown on the AlN. The thicknesses of the GaN epi-layers in (b) and (c) are 1μm and 0.750 μm, respectively.

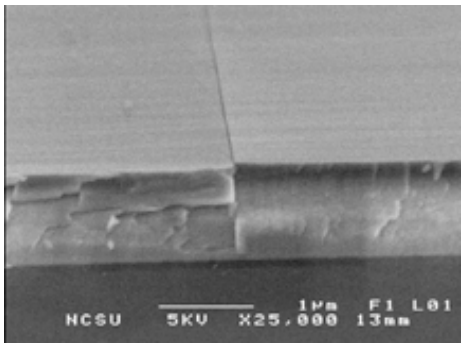

Figure 2. Cross-sectional SEM image of a cracked 1 μm thick epitaxial GaN $(11\bar{2}0)$ film grown on an AlN/4H-SiC $(11\bar{2}0)$ substrate.

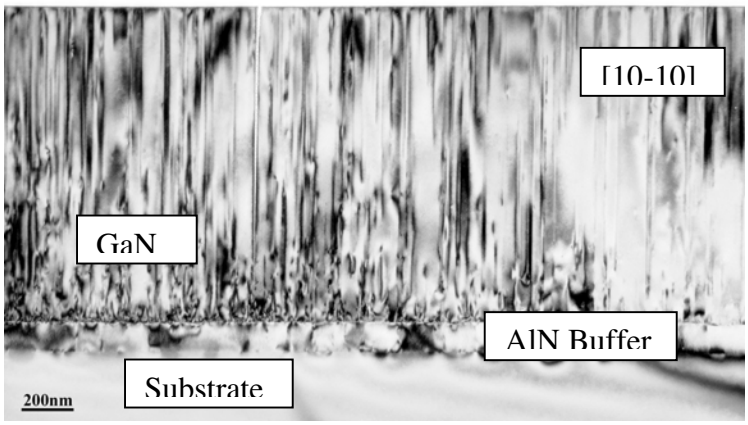

Figure 3. Cross-sectional TEM image of a GaN $(11\bar{2}0)$ film with a thickness of 1μm grown on an 0.1 μm thick AlN buffer layer deposited on a 4H-SiC $(11\bar{2}0)$ substrate.

3. Growth and Characterization of Pendeo-epitaxial GaN$(11\bar{2}0)$ on 4H-SiC$(11\bar{2}0)$ Substrates

B.P. Wagner[1], Z.J. Reitmeier[1], J.S. Park[1], D. Bachelor[2], R.F. Davis[1], D.N. Zakharov[3] and Z. Lilliental-Weber[3]

[1]Department of Materials Science and Engineering, North Carolina State University, Raleigh, NC 27695, [2]Analytical Instrumentation Facility, North Carolina State University, Raleigh, NC 27695, [3]Lawrence Berkeley National Laboratory, MS 62-203, Berkeley, CA 94720

To be submitted to the Journal of Crystal Growth

3.1 Abstract

Growth on AlN/4H-SiC$(11\bar{2}0)$ substrates of coalesced, non-polar GaN$(11\bar{2}0)$ films having volumes of material with reduced densities of dislocations and stacking faults has been achieved from etched stripes via the statistical and experimental determination of the effect of temperature and V/III ratio on the lateral and vertical growth rates of the GaN{0001} faces combined with pendeo-epitaxy. AFM of the uncoalesced GaN(0001) and GaN$(000\bar{1})$ faces revealed growth steps with some steps terminating at dislocations on the former and a pitted surface without growth steps, indicative of decomposition, on the latter. Coalescence was achieved via (a) a two-step route and the parameters of (1) T=1100ºC and V/III=1323 for 40mins. and (2) 1020ºC and V/III= 660 for 40mins. and (b) a one-step route that employed T = 1020°C and a V/III ratio = 660 for six hours. The densities of dislocations in the GaN grown vertically over and laterally from the $(11\bar{2}0)$ stripes were ~$4x10^{10}$ cm^{-2} and ~$2x10^{8}$ cm^{-2}, respectively; the densities of stacking fault in these volumes were ~$1x10^{6}$ cm^{-1} and ~$2x10^{4}cm^{-1}$, respectively. Plan view AFM also revealed different microstructures and a reduction in the RMS roughness values from 1.2nm to 0.95nm in these respective regions.

3.2 Introduction

The Group III-nitrides have become important materials for short-wavelength photonic and high-frequency devices and applications [1]. At present, the majority of the III-nitride films and device structures are grown on the (0001) plane of sapphire and SiC [2]. Gallium nitride and its alloys normally possess the wurtzite structure. The ionic contribution to the bonding in this structure gives rise to macroscopic spontaneous polarization along the <0001> polar axes. The total polarization of [0001]-oriented nitride heterostructures, e.g., AlGaN/GaN device layers, has both spontaneous and piezoelectric components [3,4]. These components produce fixed surface charges of opposite sign at the {0001} surfaces that change abruptly at every surface or hetero-interface. These polarization-induced fields have been employed for the creation of a two-dimensional electron gas in high electron mobility transistors (HEMT) [5,6]. These fields also induce electrostatic fields parallel to the c-axis [7] that spatially separate electrons and holes within quantum well structures (the quantum-confined Stark effect). This spatial separation causes a reduction in oscillator strength and a red shift in optical transitions due to a reduced quantum recombination efficiency [8] in quantum wells in III-nitride optoelectronic devices grown along the polar c-axis. To circumvent these effects, non-polar GaN-based layers have been grown and characterized on non-polar substrates including a-plane 4H-SiC $(11\bar{2}0)$ [9], r-plane sapphire $(1\bar{1}02)$ [10,11], a-plane sapphire $(11\bar{2}0)$ [12], and tetragonal (γ) $LiAlO_2$ [13]. Devices have been fabricated [14-18] on non-polar GaN-

based layers, and direct comparisons of non-polar and polar devices [19] have also been reported.

Non-polar GaN-based layers and device structures, though free of electrostatic fields, continue to be grown at this writing on the foreign substrates previously noted and contain domains, similar densities of dislocations and stacking faults in the manner of the materials grown along [0001] [20]. Dislocations in GaN (1) have energy levels in the band gap that allow carrier recombination from donor states and states at the bottom of the conduction band, (2) act as conduits for charge transport that result in high leakage currents and slow breakdown of rectifying contacts, and (3) reduce significantly the lifetime of laser diodes [1,2,21]. Several research groups have determined that lateral epitaxial overgrowth (LEO) and pendeo-epitaxy (PE) can significantly reduce the dislocation density in GaN and AlGaN films grown on sapphire(0001) [22-26] and SiC(0001) [27-35]. Further, LEO [36-38] and selective area lateral epitaxy [39] on r-plane sapphire $(1\bar{1}02)$ have been used to produce non-polar GaN-based films that posses significantly reduced densities of dislocation and stacking faults as well as surface microstructures free of pits and other defects derived from anisotropic growth in the $(11\bar{2}0)$ plane [40,41].

The principal objective of the research reported herein has been the growth of non-polar of GaN $(11\bar{2}0)$ films via pendeo-epitaxy (PE) on 4H-SiC $(11\bar{2}0)$ substrates and characterization of the surface and defect microstructures.

3.3 Experimental Procedure

The epitaxial AlN buffer layers, the subsequently deposited epitaxial GaN seed films and the PE GaN layers were grown in-situ in a cold-wall, vertical, pancake-style metalorganic vapor phase epitaxy (MOVPE) system on research grade, on-axis 4H-SiC$(11\bar{2}0)$ substrates which had been previously etched in a 10% HF solution to remove the native oxide. The design of the reactor was originally modeled via finite element analysis and constructed to produce a high velocity laminar flow without recirculation above the substrate. This resulted in the growth of two-inch diameter AlN and GaN films with a thickness variance of 0.7%. The substrates were seated in a 2" diameter pocket centered in a rotating SiC-coated graphite platter beneath which was located a DC resistive graphite heater. The radial temperature gradient was 10±5°C. During growth the temperature was measured at the edge of the pocket using an optical pyrometer. The 100 nm thick AlN buffer layers and the 500 nm thick GaN seed layers were grown at 20 Torr and platter temperatures of 1100°C and 1020°C, respectively. The precursor species (mass flow rates) of tri-methylaluminum (TMA; 5.4μmol/min carried in H_2), tri-ethylgallium (TEG; 101μmol/min carried in H_2) and ammonia (NH_3; 0.14mol/min) were mixed with a high-purity H_2 diluent (3 slm) in a two-inch internal diameter sleeve located approximately five centimeters above the substrate.

A Ni layer was deposited on patterned photoresist stripes on each GaN seed layer by e-beam evaporation. Etch mask stripes were subsequently produced using standard photolithography lift-off techniques. An inductively coupled plasma (ICP) system and a mixture of Cl_2 and BCl_3 gases at a 9:1 ratio were used to etch the

unmasked striped regions through the GaN and the AlN layers and into the near-surface regions of the SiC substrate. The Ni was then removed using a 5 min dip in 50% HNO_3. The remaining GaN seed layer consisted of 3 μm wide stripes and 3 μm separations oriented along $[1\bar{1}00]$. The separations or stripes were oriented along the $[1\bar{1}00]$ direction for two reasons. Firstly, the nature of the basal-plane stacking faults in GaN $(11\bar{2}0)$ thin films, characterized by Zakharov et al [20], should not propagate into laterally grown GaN with stripes oriented in the $[1\bar{1}00]$ direction. Secondly, Craven et al [36] demonstrated that in LEO GaN with the windows with $[1\bar{1}00]$ orientation, threading dislocations did not bend into the laterally grown GaN. Figure 1 is an SEM micrograph showing the GaN stripes after the ICP etch, but before the GaN re-growth. The exposed (0001) sidewalls and the top $(11\bar{2}0)$ faces of the stripes were subsequently dipped in 50% hot HCl to clean the surface prior to regrowth of the PE layer.

The lateral and vertical growth rates of the PE GaN films were very sensitive to temperature and the NH_3/TEG (V/III) molar flow rate ratios. Initial experimental measurements of the lateral growth rates from the Ga- and N- terminated {0001} sides of the stripes and the vertical growth rate from the $(11\bar{2}0)$ top plane of the stripes were acquired from SEM micrographs before and after growth at selected temperatures and V/III ratios determined by a design of experiments via use of a statistical analysis software (JMP) with experimental design capabilities, employing an n=2 full factorial design with a center point. These data were subsequently used in tandem with the DOE software to predict the effect of changes in V/III ratio and

temperature within the ranges of 1323-to-2646 and 1020°C-to-1100°C, respectively, on the lateral and vertical growth rates of the GaN.

The respective microstructures of the {0001} and $(11\bar{2}0)$ pendeo-epitaxial surfaces of the uncoalesced and coalesced GaN films were determined via atomic force microscopy (AFM) in the tapping mode using a Digital Instruments D3000 AFM with a silicon tip. Cross-sectional and plan-view images of the PE GaN before and after coalescence were also obtained using SEM (JEOL 6400 FE). Cross-sectional and plan-view samples were prepared for transmission electron microscopy (TEM) and high resolution electron microscopy (HREM) using the sequence of mechanical polishing, dimpling to a thickness of 10μm and argon ion milling at 5kV until perforation. The TEM and HREM studies utilized a JEOL 3010 microscope operated at 300kV to acquire the necessary images.

The following Sections present and discuss the results of the effect of temperature and V/III ratio on the lateral and vertical growth rates of GaN from the {0001} sidewalls of the $[1\bar{1}00]$-oriented stripes and the achievement of coalesced $(11\bar{2}0)$ oriented films of this material.

3.4 Results and Discussion

SEM studies revealed that both the (0001) and the $(000\bar{1})$ sidewalls of the GaN/AlN/SiC stripes (a.k.a. seeds) produced via ICP etching sloped away from the normal to the substrate surface, changed slope at the AlN/SiC interface within the stripes and exhibited vertically-oriented scalloping, as shown in Figures 1 (a) and (b).

By contrast, the etched $(11\bar{2}0)$ surfaces of the SiC were smooth and featureless. The results of subsequent SEM studies such as those shown in Figure 2 indicated that neither the microstructure nor the morphology nor the rate of lateral regrowth from these stripes of uncoalesced GaN films was affected by the initial microstructures and slopes within the stripes. The morphology and microstructure of the stripes shown in Figures 1 (a) and (b) are representative of those used in all the studies discussed in the following paragraphs.

The data presented in Table 1 indicates the sensitivity of the vertical growth rate (V) from the $(11\bar{2}0)$ surface, the lateral growth rate of the Ga-terminated (0001) face (Lg), the lateral growth rate of the N-terminated $(000\bar{1})$ face (Ln), the ratio Rg (Lg/V) and the ratio Rn (Ln/V) to combinations of T and the NH_3/TEG (V/III) molar flow rate ratio and to changes in these combinations. The growth rates shown in this Table were calculated by comparing the positions of the {0001} sidewalls and the $(11\bar{2}0)$ surface in SEM micrographs acquired before and after GaN regrowth and were used in the statistical analysis appropriate to the selected experimental design.

The results of the DOE study revealed distinct trends in the critical statistical analysis. The factors of temperature and V/III ratio were significant to the five response variables analyzed (V, Lg, Ln, Rg, and Rn); however, the interactions between these two factors were not found to be statistically significant. An analysis of f-ratios showed the V/III ratio to be more influential than temperature in all the response variables. The DOE results predicted that increasing either the temperature or the V/III ratio would cause a decrease the values of Rg and Lg and an increase the values of Rn, Ln, and V. Stated another way, lower temperatures and/or V/III ratios

would suppress vertical growth rates, while increasing the lateral growth rate along the [0001] direction. Use of the information provided by the DOE studies allowed coalescence of non-polar GaN thin films to be realized via two different routes, as described in the following paragraphs.

The SEM micrographs shown in Figures 2 (a) and (b) of the cross-sections of representative stripes of the uncoalesced pendeo-epitaxial samples reveal the material characteristics resulting from the use of a two-step process having the growth parameters of (1) low temperature (1020ºC) and an intermediate V/III ratio (1323) for 40 minutes and (2) high temperature (1100ºC), and an intermediate V/III ratio (1323) for 40 minutes, respectively. These micrographs and those presented in Figure 3 ~~also~~ show that the growth rate in the Ga-polar [0001] direction is significantly faster than that in the N-polar $[000\bar{1}]$ direction. Wu et al. [42] observed similar polarity effects in GaN $(11\bar{2}0)$ sidewalls grown laterally from $[1\bar{1}00]$-oriented stripes using the LEO process. These results also provide the explanation for the space between the [0001]–oriented AlN/SiC substrates and the $(000\bar{1})$ surface of III-Nitride films grown via pendeo-epitaxy, the observation of which suggested the name for this growth process [33-35].

Figures 3 (a) and (b) show TEM micrographs acquired from an uncoalesced pendeo-epitaxial sample grown for 40 minutes under the conditions of T = 1020°C and a V/III ratio = 1323, i.e., the conditions used in the growth of the sample shown in Figure 2(a). The values of g = [0002] and $[1\bar{1}00]$ in (a) and (b), respectively. The dislocation densities within the seed and wing regions are 4.4×10^{10} cm^{-2} and within the range of 2×10^{8} cm^{-2} to 1×10^{9} cm^{-2}, respectively. The latter range of values is due

to a variation in dislocation density within each wing region (see below) and from wing-to-wing. The stacking fault densities in the seed and wing regions are 1.0×10^6 cm^{-1} and $2.3 \times 10^4 cm^{-1}$, respectively. The occurrence of stacking faults is somewhat surprising, as they had not been observed in either our conventional or our pendeo-epitaxial [0001]–oriented GaN films grown on 6H-SiC(0001) substrates. As expected, the wing regions contain reduced densities of dislocations and stacking faults in comparison to both the seed regions of the sample and to other reported [9-12] values of dislocation density in GaN$(11\bar{2}0)$ films where no lateral growth techniques were employed. The wing regions also contain large areas where dislocations are not observed; this is equivalent to a density of $\sim 1 \times 10^6$ cm^{-2}, the lowest reasonable value for this metric that can be determined from a few TEM micrographs. However, a few dislocations can be observed to propagate into portions of the wing regions, as indicated by the arrow in Figure 3 (a) and, in some cases, intersect with the advancing (0001) surface of the GaN.

An AFM micrograph of an uncoalesced GaN(0001) sidewall in a sample grown under the same conditions employed to obtain the material characterized by TEM (see Figure 3) is shown in Figure 4. Growth steps in tandem with steps terminating at defects intersecting the growth surface are apparent in the 1.5μm x 1.5μm scan shown in Figure 4. This is a commonly observed microstructure for [0001]-oriented GaN films heteroepitaxially grown on Al-polar AlN/SiC(0001) substrates [43]. The RMS roughness of the microstructure, from a large area scan not shown in Figure 4, is 0.420nm. The micrograph of the 1.5μm x 1.5μm scan shown in Figure 4 was acquired from the bottom of the wing shown in Figure 3 with the top of

Figure being closest to the SiC substrate. As such, it is representative of the initially deposited material closest to the SiC substrate. The dislocation density of the material shown in Figure 4(b) is ~1.5×10^9 cm^{-2}, which is within the range measured from TEM micrographs that contain this area such as those shown in Figure 3. However the distribution of the dislocations is non-uniform. The upper 0.50μm of the scan in Figure 4 shows many dislocations intersecting the surface, as indicated in the micrograph by the black spots. The large black spot in the upper right corner is either a pore or a collection of dislocations having screw or mixed character that have intersected the growth surface. The clockwise curvature and apparent cessation of the adjacent steps suggest that the latter defects explain this feature. By contrast, dislocations were not observed to intersect the surface shown in the lower 1μm of this AFM micrograph. This observation, in tandem with the TEM micrographs in Figure 3, also indicate that the [0001]-oriented GaN wings contained moderate volumes of essentially dislocation-free material.

Figure 5 shows AFM micrographs of the N-polar $(000\bar{1})$ face of the GaN sample shown in Figure 4. The Figure 5 micrograph is inverted in the same manner as Figure 4. The RMS roughness of the microstructure, from a large area scan not shown in Figure 5, is 0.617nm. This value is similar to that determined for the (0001) face; however, neither growth steps nor the intersection of dislocations with the surface were observed on the $(000\bar{1})$ face. By contrast, the microstructure shown in Figure 5(b) reveals a pitted and decomposed surface. Wu, et al. [42] observed via SEM hillock features on the $(000\bar{1})$-face. Surface decomposition was not reported.

The achievement of coalescence between the $(000\bar{1})$ and (0001) surfaces growing from GaN$(11\bar{2}0)$ stripes in this research was markedly more challenging than the analogous coalescence of GaN$\{11\bar{2}0\}$ surfaces growing from GaN(0001) stripes [27-35]. Comparison of the initial lateral growth rates achieved under the various sets of conditions denoted in Table 1 indicated that the growth regime used to grow the uncoalesced sample shown in Figure 2(a), namely, T = 1020°C and a V/III ratio = 1323 should be employed at the outset to coalesce the laterally growing (0001) faces in the shortest period. However, coalescence was not achieved after 3 hours, and the diagonal facet shown in Figure 2(a) formed again.

The cross-section of the uncoalesced stripe presented in Figure 2(b) shows that the use of the growth conditions of 1100ºC and V/III=1323 results in an unfaceted, rectangular growth profile. Moreover, the nitrogen face had a very small but measurable growth rate, as indicated in Table 1. As such, it was reasoned that a two-step approach that incorporated in the same growth run both sets of conditions used to grow the samples shown in Figures 2(a) and (b) should be investigated to achieve coalescence. The etched GaN sample was initially heated under the conditions of T = 1020°C and V/III ratio = 1323 for 1.5 hours and subsequently at T = 1100ºC and V/III ratio = 1323 for 1.5hrs. In essence, this was an attempt to coalesce the GaN via (1) the rapid growth of the (0001) face and the eventual elimination of the growth facet and (2) the simultaneous growth of the GaN$(000\bar{1})$ face towards the GaN(0001) face. However, heating the sample to 1100ºC caused decomposition of the GaN$(000\bar{1})$ face in a manner similar to that shown in Figure 6(a), and coalescence was not achieved.

A second, dual step approach was explored, namely, (1) growth at T = 1100ºC and a V/III ratio =1323 for 1.5 hrs. to achieve the rectangular cross-sectional morphology shown in Figure 2(b), followed by a reduction in the temperature and V/III ratio to 1020ºC and 660, respectively, for 1.5 hrs. to increase the growth rate of the {0001} faces. The V/III ratio of 660 was chosen because the DOE calculations predicted increased growth rates for the {0001} faces at low ratios. This approach proved successful after 3μm and 7μm of lateral and vertical growth, respectively. Cross-sectional and plan-view SEM micrographs of these microstructures are shown in Figures 6(a) and (b), respectively. The two-step process to coalescence was achieved with a modicum of lateral growth of the GaN$(000\bar{1})$ surfaces. However, examination of the right-hand edge of each vertical cavity of the film in Figure 6(a) reveals that some decomposition of these surfaces also occurred. The plan-view micrograph presented in Figure 6(b) reveals a relatively rough top surface that contains growth fronts that have not completely coalesced. The regions of coalesced material were small in comparison to the regions in Figure 6(b). As such, an alternate one-step approach was investigated.

As mentioned previously, the DOE results indicated that the use of low temperatures and low V/III ratios would increase the lateral growth rate of the (0001) face relative to that of the $(11\bar{2}0)$ surface. The results of studies in this laboratory by Nam and coworkers [44] of the effects of temperature and V/III ratio on the lateral/vertical growth rate ratio and the resulting morphology of uncoalesced GaN(0001) films grown using the LEO process also suggested that this approach would enhance the lateral growth rate of the (0001) face (or at least reduce the growth

rate of the $(11\bar{2}0)$ surface). As such, the temperature and V/III ratio for the one-step approach were set at 1020ºC and 660, respectively. Under these conditions coalescence of the upper volume of GaN was achieved over most of the sample after six hours and approximately 3μm and 5μm of lateral and vertical growth, respectively. The coalescence was accomplished almost solely via the advance of the (0001) surfaces. Cross-sectional and plan-view SEM micrographs of this film are shown in Figures 7(a) and (b), respectively. Figure 7(a) again shows that decomposition occurred on the $(000\bar{1})$ surface (left side) of each vertical cavity. Essentially all the top surface of the coalesced GaN material was smooth and featureless. The small particles shown in Figure 7(b) were used for focusing, and were not characteristic of the coalesced surface.

The results of companion TEM studies on the material from which Figure 7 was obtained revealed striking microstructural differences between the GaN that grew directly above the etched stripes and that which grew laterally. Figure 8(a) is a cross sectional image of three coalesced regions; the areas where the laterally growing GaN were joined are indicated by the dashed arrows located directly above the apex of each vertical void. Figure 8(b) shows a bright field TEM image recorded using a two-beam condition and the g-vector of $[1\bar{1}00]$ which is close to the $[11\bar{2}0]$ zone-axis. This imaging condition allowed the observation of the edges of the basal-plane stacking faults (BSF) that either grew from those present in the etched stripes or formed within the material that grew above these stripes. Threading dislocations were also observed; they were primarily partial dislocations that terminated the BSF's. The density of the BSF's (threading dislocations) decreased from

~1.3×10^{6}cm^{-1} (~4.2×10^{10}cm^{-2}) in the GaN that grew directly above the stripes to ~1.2×10^{4} cm^{-1} (~1.0×10^{8}cm^{-2}) in the laterally grown material. The densities of both of these defects varied slightly within the laterally grown volumes. Craven et al. [36,45] reported similar TEM results for LEO GaN $(11\bar{2}0)$ showing a reduction in BSF's and threading dislocations for windows oriented in the $[1\bar{1}00]$ direction. The density of the threading dislocations observed in the laterally grown and coalesced GaN in Figure 8 was approximately the same as that observed in the laterally grown and uncoalesced material shown in Figure 3.

The 20μm x 20μm AFM scan of the coalesced GaN surface of the sample shown in Figure 7 is presented in Figure 9(a) and shows similar seed and wing regions to those presented in Figures 7(b) and 8(b). The RMS roughness for the area shown in this Figure is 6.4 nm. Figures 9(b) and (c) show 5.0μm x 5.0μm and 2.0μm x 2.0μm scans, respectively, of the same region shown in 9(a). The RMS roughness of the seed and wing regions were 1.2nm and 0.95nm, respectively, i.e., the roughness of the latter was ~25% lower than that of the former. Further, Figure 9(c) gives an even better representation of the microstructural difference between the seed and wing regions of the sample. The dark spots in the seed regions in Figures 9(b) and (c) have a density of approximately 2.5×10^{9} cm^{-2}, which agrees with the values of the dislocation density in this region calculated from TEM micrographs. It is reasonable to conclude that the difference in the surface microstructure between the seed and wing GaN material are largely due to different densities of threading dislocations in the two areas and that the dark spots/micropits decorate the points where the threading dislocations intersect the surface. Haskell et al [37] reported similar AFM

results for HVPE LEO GaN $(11\bar{2}0)$. The RMS values for the wing and window in this latter study were 0.9nm and 1.3nm, respectively. AFM micrographs revealed micropits that decorated threading dislocations that intersected the surface in densities of of $3x10^6$ cm^{-2} and $\sim10^9$ cm^{-2} in the wing and window areas, respectively, in this material.

3.5 Conclusions

- Lateral and vertical growth from etched stripes of $(11\bar{2}0)$-oriented non-polar GaN films previously deposited on AlN/4H-SiC $(11\bar{2}0)$ substrates and subsequent coalescence of the GaN via pendeo-epitaxy has been accomplished through the statistical and experimental determination of the effect of growth temperature and V/III ratio on the growth rates of the (0001) and $(000\bar{1})$ GaN faces.
- AFM of the uncoalesced GaN(0001) and GaN $(000\bar{1})$ faces revealed growth steps with some steps terminating at dislocations intersecting the surface in the former and a pitted surface without growth steps, indicative of decomposition, in the latter.
- Two routes to coalescence were determined: (1) a two-step process having the parameters of (a) T=1100ºC and V/III=1323 for 1.5 hrs and (b) 1020ºC and V/III= 660 for 1.5 hrs and (2) a one-step process with the parameters of T = 1020°C, V/III ratio = 660 and time = 6 hrs.

- TEM revealed that the densities of dislocations in the volumes of GaN grown vertically (seed material) and laterally (wing material) from the stripes were ~$4.2 \times 10^{10} cm^{-2}$ and ~$2.0 \times 10^{8} cm^{-2} cm^{-2}$, respectively; the respective densities of the stacking faults in these same volumes were ~$1.3 \times 10^{6} cm^{-1}$ and ~1.2×10^{4} cm^{-1}.

3.6 References

[1] S.J. Pearton, J.C. Zolper, R.J. Shul, F. Ren, *J. Appl. Phys.* **86** (1999) 1.

[2] S.C. Jain, M. Willander, J. Narayan, R. Van Overstraeten, *J. Appl. Phys.* **87** (2000) 965.

[3] F. Bernardini, V. Fiorentini, *Phys. Rev. B* **56** (1997) R10024.

[4] F. Bernardini, V. Fiorentini, *Phys. Rev. B* **57** (1998) R9427.

[5] I.P. Smorchkova, C.R. Elsass, J.P. Ibbetson, R. Vetury, B. Heying, P. Fini, E. Haus, S.P. DenBaars, J.S. Speck, U.K. Mishra, *J. Appl. Phys*. **86** (1999) 4520.

[6] O. Ambacher et al, *J. Appl. Phys.* **85** (1999) 3222.

[7] T. Takeuchi, S. Sota, M. Katsurgawa, M. Komori, H Takeuchi, H. Amano, I. Akasaki, *Jpn. J. Appl. Phys.* Part 2 **36** (1997) L382.

[8] J.S. Im, H. Kollmer, J. Off, A. Sohmer, F. Scholz, A. Hangleiter, *Phys. Rev. B* **57** (1998) R9435.

[9] B.P. Wagner, E.A. Preble, Z.J. Reitmeier, R.F. Davis, D.N. Zakharov, Z. Liliental-Weber, *Mat. Res. Soc. Symp. Proc.* **798** (2004) Y10.34.1.

[10] M.D. Craven, S.H. Lim, F. Wu, J.S. Speck, S.P. DenBaars, *Appl. Phys. Lett.* **81** (2002) 469.

[11] B.A. Haskell, F. Wu, S. Matsuda, M.D. Craven, P.T. Fini, S.P. DenBaars, J.S. Speck, S. Nakamura, *Appl. Phys. Lett.* **83** (2003) 1554.

[12] Sugianto, R.A. Sani, P. Arifin, M. Budiman, M. Barwami, *J. Crystal Growth* **221** (2000) 311.

[13] P. Waleriet, O. Brandt, A. Trampert, H.T. Grahn, J. Menninger, M. Rammsteiner, M. Reiche, K.H. Ploog, *Nature* **406** (2000) 865.

[14] C. Chen, V. Adivarahan, J. Yang, M. Shatalov, E. Kuoksis, M.A. Khan, *Jpn. J. Appl. Phys.* **42** (2003) L1039.

[15] V. Adivarahan, C. Chen, J. Yang, M. Gaveski, M. Shatalov, G. Simin, M.A. Khan, *Jpn. J. Appl. Phys.* **42** (2003) L1136.

[16] W.H. Sun et al., *Appl. Phys. Lett.* **83** (2003) 2599.

[17] H.M. Ng, A. Bell, F.A. Ponce, S.N.G. Chu, *Appl. Phys. Lett.* **83** (2003) 653.

[18] S. Iyer, D.J. Smith, A. Bhattacharyya, K. Ludwig Jr., T.D. Moustakas, *Mat. Res. Soc. Symp. Proc.* **743** (2003) L3.20.1.

[19] E. Kuokstis et al., *Appl. Phys. Lett.* **81** (2002) 4130.

[20] D.N. Zakharov, Z. Liliental-Weber, B.P. Wagner, Z.J. Reitmeier, E.A. Preble, R.F. Davis, *Mat. Res. Soc. Symp. Proc.* **798** (2004) Y5.28.1.

[21] S.Nakamura, M. Senoh, S.I. Nagahama, T. Matushita, K. Kiyoku, Y. Sugimoto, T. Kozaki, H. Umemoto, M. Sano, T. Mukai, *Jpn. J. Appl. Phys*., Part 2 **38** (1999) L226.

[22] D. Kapolnek, S. Keller, R. Vetury, R.D. Underwood, P. Kozodoy, S.P. DenBaars, U. K. Mishra, *Appl. Phys. Lett.* **71** (1997) 1204.

[23] H. Marchand, J.P. Ibbetson, P.T. Fini, S. Chichibu, S.J. Rosner, S. Keller, S.P. DenBaars, J.S. Speck, U. K. Mishra, in *25th Int. Symp. Compound. Semiconductors.* IOP Publishing, Nara, Japan, 1998, p. 681.

[24] H. Kim, C. Sone, O.H. Nam, Y.J. Park, T. Kim, *Appl. Phys. Lett.* **75** (1999) 4109.

[25] Sakai, H. Sunakawa, A. Kimura, A. Usui, *Appl. Phys. Lett.* **76** (2000) 442.

[26] X. Zhang, P.D. Dapkus, and D. H. Rich, *Appl. Phys. Lett.* **77** (2000) 1496.

[27] A.M. Roskowski, E.A. Preble, S. Einfeldt, P.M. Miraglia, J. Schuck, R. Grober, R.F. Davis, *Opto-electronics Review* **10** (2002) 261.

[28] O. H. Nam, M.D. Bremser, T.S. Zheleva, R. F. Davis, *Appl. Phys. Lett.* **71** (1997) 2638.

[29] O. H. Nam, T. S. Zheleva, M.D. Bremser, R. F. Davis, *J. Elect. Mater.* **27** (1998) 233.

[30] R. F. Davis, T. Gehrke, K.J. Linthicum, T.S. Zheleva, E.A. Preble, P. Rajagopal, C.A. Zorman, M. Mehregany, *J. Cryst. Growth* **225** (2001) 134.

[31] R. S. Q. Fareed, J. W. Yang, J. Zhang, V. Adivarahan, V. Chaturvedi, M. A. Khan, *Appl. Phys. Lett.* **77** (2000) 2343.

[32] T. Gehrke, K.J. Linthicum, E. Preble, P. Rajagopal, C. Ronning, C. Zorman, M. Mehregany, R. F. Davis, *J. Electron. Mater.* **29** (2000) 306.

[33] K. Linthicum, T. Gehrke, D. Thomson, E. Carlson, P. Rajagopal, T. Smith, D. Batchelor, R. F. Davis, *Appl. Phys. Lett.* **75,** (1999) 196.

[34] D. B. Thomson, T. Gehrke, K.J. Linthicum, P. Rajagopal, R. F. Davis, *MRS Internet J. Nitride Semicond. Res.* **4S1** (1999) G3.37.

[35] T. Zheleva, S. Smith, D. Thomson, K. Linthicum, *J. Electron. Mater.* **28** (1999) L5-L8.

[36] M.D. Craven, S.H. Lim, F. Wu, J.S. Speck, S.P. DenBaars, *Appl. Phys. Lett.* **81** (2002) 1201.

[37] B.A. Haskell, F. Wu, M.D. Craven, S. Matsuda, P.T. Fini, T. Fujii, K. Fujito, S.P. DenBaars, J.S.Speck, S. Nakamura, *Appl. Phys. Lett.* **83** (2003) 644.

[38] C. Chen, J. Yang, H. Wang, J. Zhang, V. Adivarahan, M. Gaveski, E. Kuokstis, Z. Gong, M. Su, M.A. Khan, *Jpn. J. Appl. Phys.* **42** (2003) L640.

[39] C. Chen et al., *Jpn. J. Appl. Phys.* **42** (2003) L818.

[40] D.S. Li, H. Chen, H.B. Yu, X.H. Zheng, Q.Huang, J.M. Zhou, *J. Crystal Growth* **265** (2004) 107.

[41] H. Wang, C. Chen, J. Zhang, M. Gaevski, M. Su, J. Yang, M.A. Khan, *Appl. Phys. Lett.* **84** (2004) 499.

[42] F. Wu, M.D. Craven, S.H. Lim, J.S. Speck, *J. Appl. Phys.* **94** (2003) 942.

[43] H.X. Liu, G.N. Ali, K.C. Palle, M.K. Mikhov, B.J. Skromme, Z.J. Reitmeier, R.F. Davis, *Mat. Res. Soc. Symp. Proc.* **743** (2002) 381.

[44] O. H. Nam, M. D. Bremser, B. L. Ward, R. J. Nemanich and R. F. Davis, *Jap. J. Appl Phys, Part 2-Letters* **36** (1997) L532.

[45] M.D. Craven, S.H. Lim, F. Wu, J.S. Speck, and S.P. DenBaars, *Phys. Stat. Sol. (a)* **194** (2002) 541.

3.7 Tables

Table 1: Results of DOE studies with n=2 full factorial with a center-point to determine the effect of temperature and V/III ratio on the growth rate of GaN vertically from the $(11\bar{2}0)$ surface (V) and laterally from both the Ga-terminated (0001) face (Lg) and the N-terminated $(000\bar{1})$ face (Ln) and on the ratios Rg (Lg/V) and Rn (Ln/V).

Temperature (°C)	**V/III (TEG/NH_3)**	**V (μm/hr)**	**Lg (μm/hr)**	**Ln (μm/hr)**	**Rg = (Lg/V)**	**Rn = (Ln/V)**
1020	1323	1.430	2.392	0.000	1.134	0.000
1100	1323	2.130	1.563	0.392	0.736	0.182
1020	2646	1.535	0.550	0.576	0.246	0.256
1100	2646	2.187	0.000	0.985	0.000	0.303
1060	1984.5	2.013	0.224	1.031	0.077	0.345

3.8 Figures

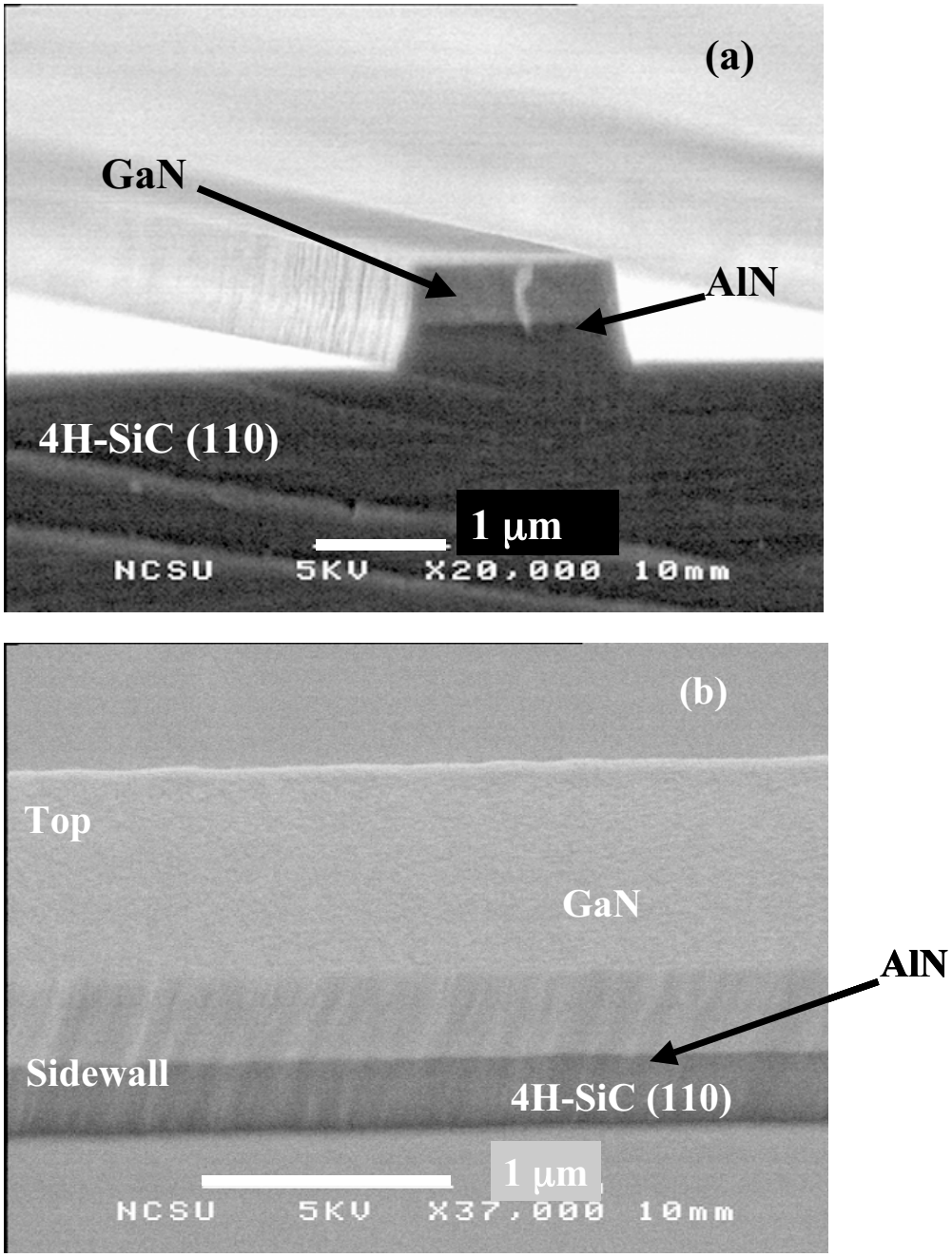

Figure 1: SEM micrographs showing (a) the cross section and (b) the top and sidewall of a representative GaN stripe, produced via ICP etching, and used as a template for pendeo-epitaxial re-growth of a GaN film.

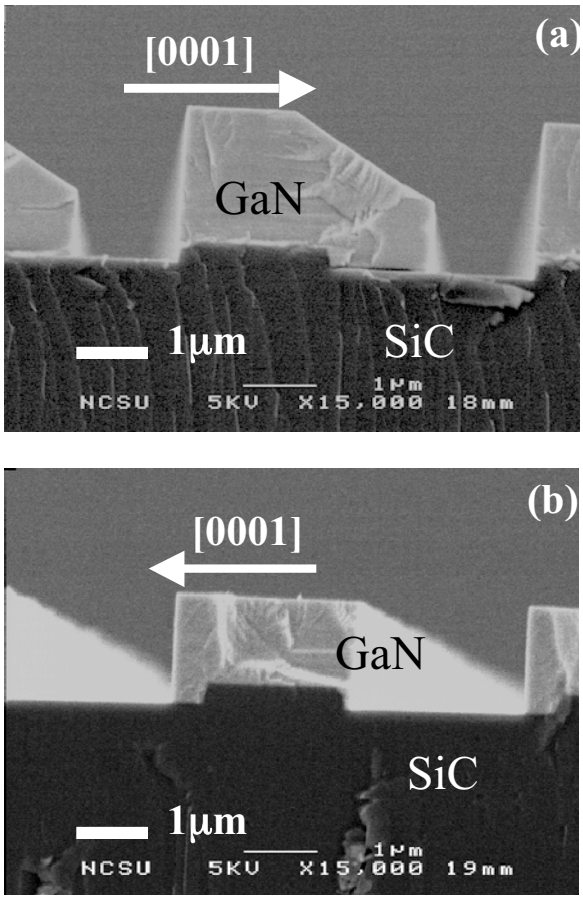

Figure 2: SEM micrographs (15,000x) of uncoalesced pendeo-epitaxial samples that exhibit the growth characteristics and features resulting from the use of growth parameters involving (a) low temperature (1020ºC) and an intermediate V/III ratio (1323) for 40 mins. and (b) high temperature (1100°C) and an intermediate V/III ratio (1323) for 40 mins.

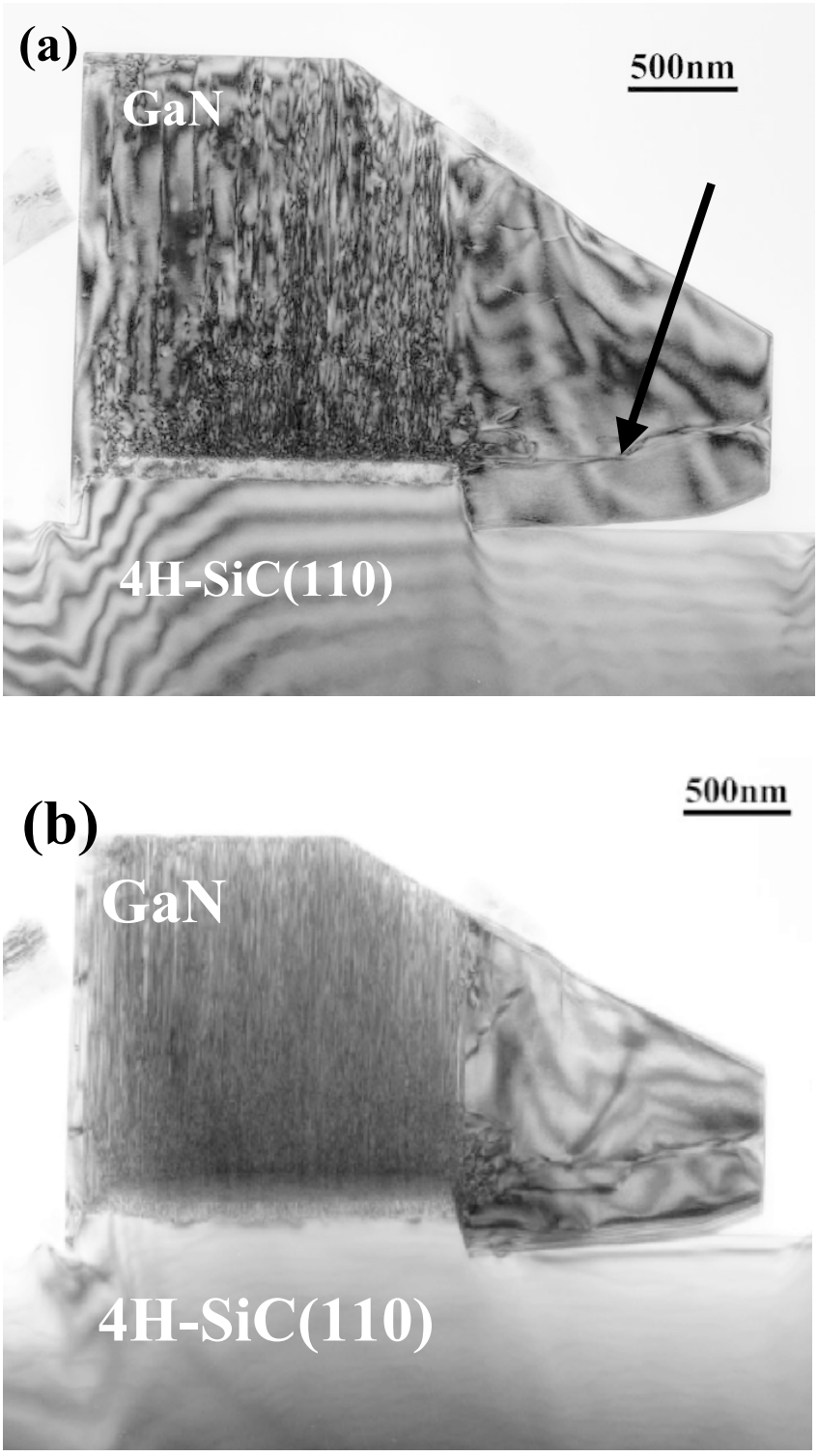

Figure 3: (a) and (b) show TEM micrographs acquired from an uncoalesced sample grown at 1020°C using a V/III ratio = 1323 for 40 mins. g = [0002] and $[1\bar{1}00]$ in (a) and (b), respectively. The arrow in (a) indicates a dislocation that has propagated into the wing.

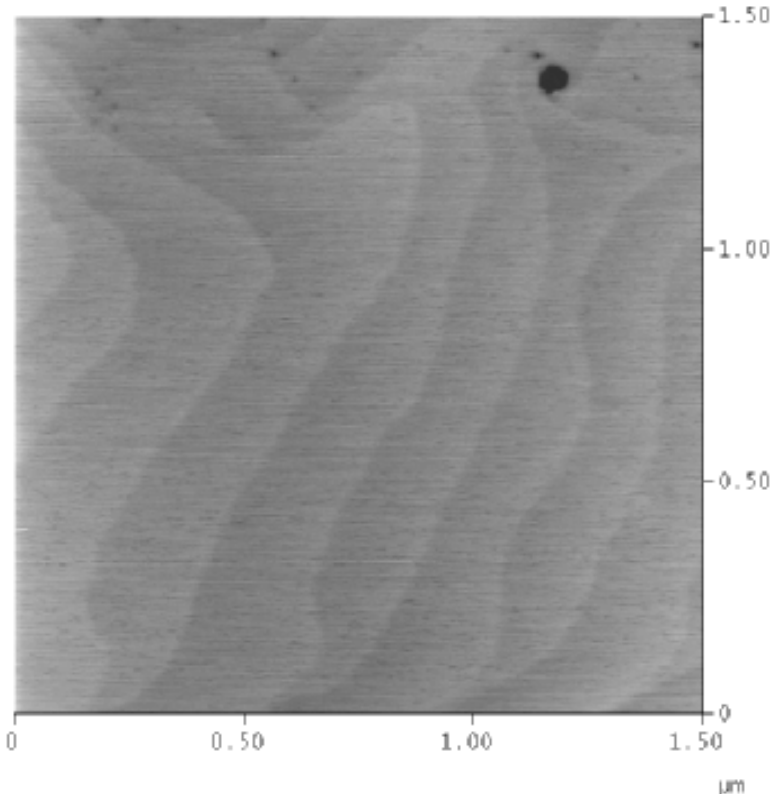

Figure 4: 1.5 µm x 1.5 µm AFM micrograph showing steps on the (0001) sidewall of an uncoalesced GaN film grown under the same conditions as the material used to produce Figure 3 and with an RMS roughness of 0.420nm. The micrograph is inverted, i.e., the material at the top of the micrograph was deposited nearest to the 4H-SiC $(11\bar{2}0)$ substrate. The black specks in the top 500nm of the micrograph are indicative of the intersection of dislocations with the growing surface. The dislocation density is 1.5×10^{9} cm^{-2}.

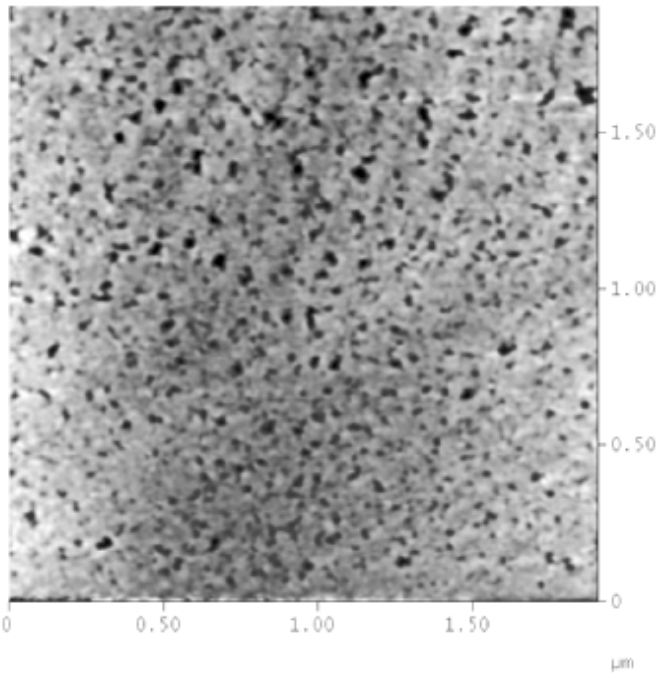

Figure 5: 2.0 µm x 2.0 µm AFM micrograph of an uncoalesced, pitted and decomposed GaN($000\bar{1}$) sidewall acquired from the sample shown in Figure 4. The micrograph is inverted, i.e., the material at the top of the micrograph was deposited nearest to the 4H-SiC ($11\bar{2}0$) substrate. The RMS roughness is 0.617nm.

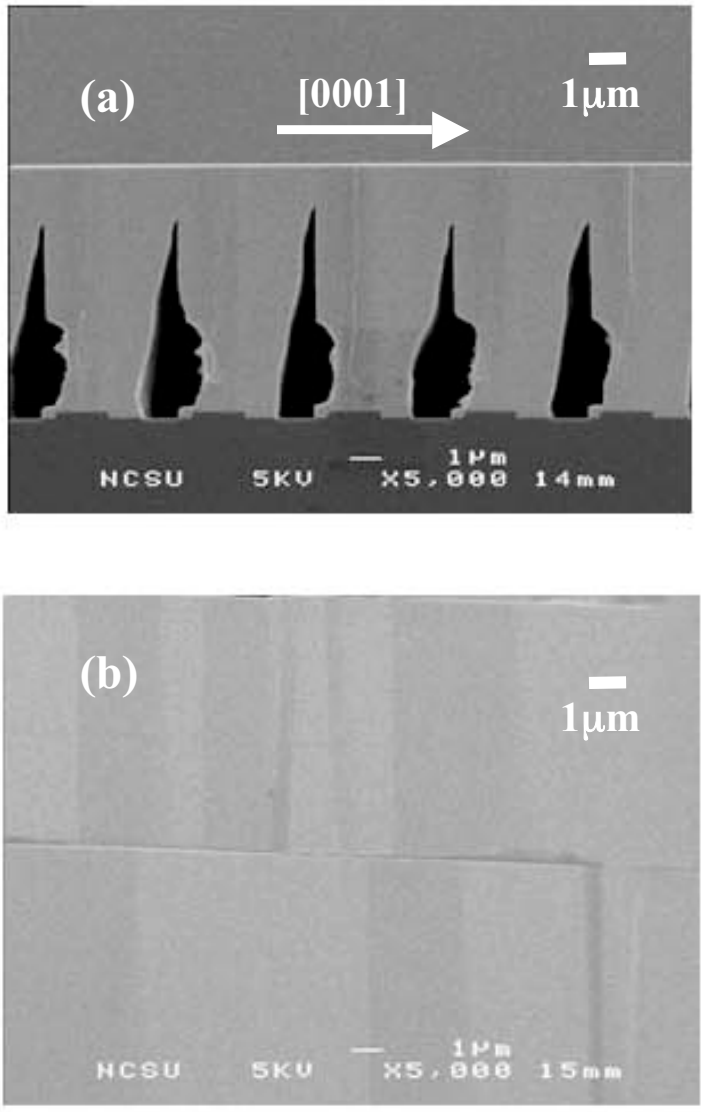

Figure 6: (a) Cross-sectional and (b) plan view SEM micrographs showing a coalesced region of pendeo-epitaxial GaN achieved using a two-step process route, namely, (1) T=1100ºC and V/III=1323 for 40 mins. and (2) 1020ºC and V/III= 660 for four hrs. Note the decomposition on each GaN($000\bar{1}$) surface in the vertical cavities in (a).

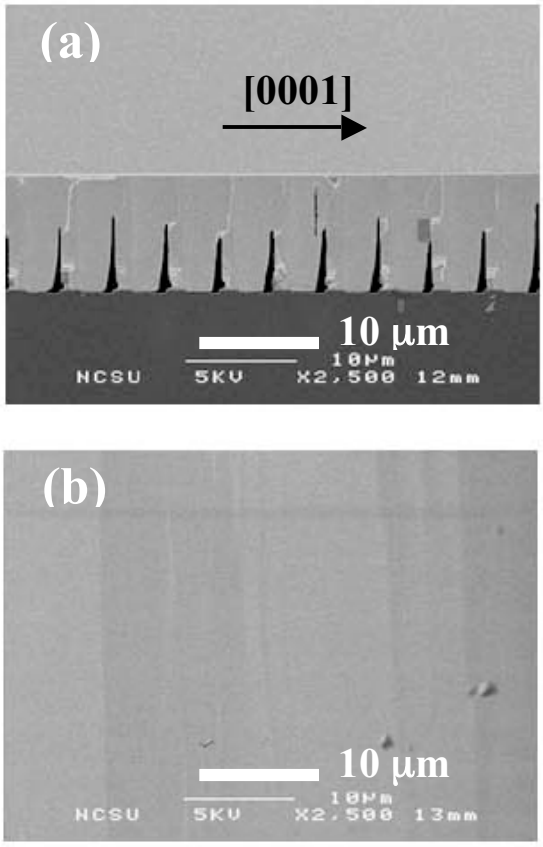

Figure 7: (a) Cross-sectional and (b) plan view SEM micrographs showing coalesced pendeo GaN achieved using the growth conditions of T = 1020ºC and V/III ratio = 660 for six hours. Note the decomposition on each GaN($000\bar{1}$) surface in the vertical cavities shown in (a).

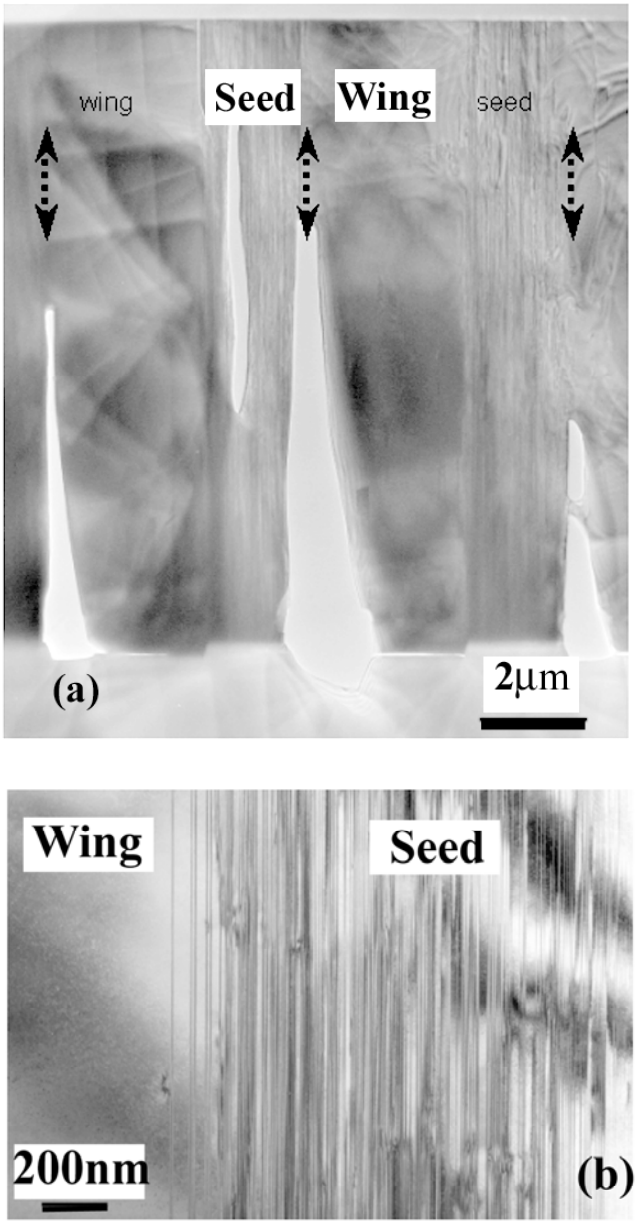

Figure 8: (a) Cross-sectional and (b) plan view TEM micrographs of the coalesced pendeo-epitaxial sample shown in Figure 7 was acquired. The g-vector in (b) is $[1\bar{1}00]$ which is close to the $[11\bar{2}0]$ zone-axis. The [0001]-oriented defects in the "seed" region are basal plane stacking faults.

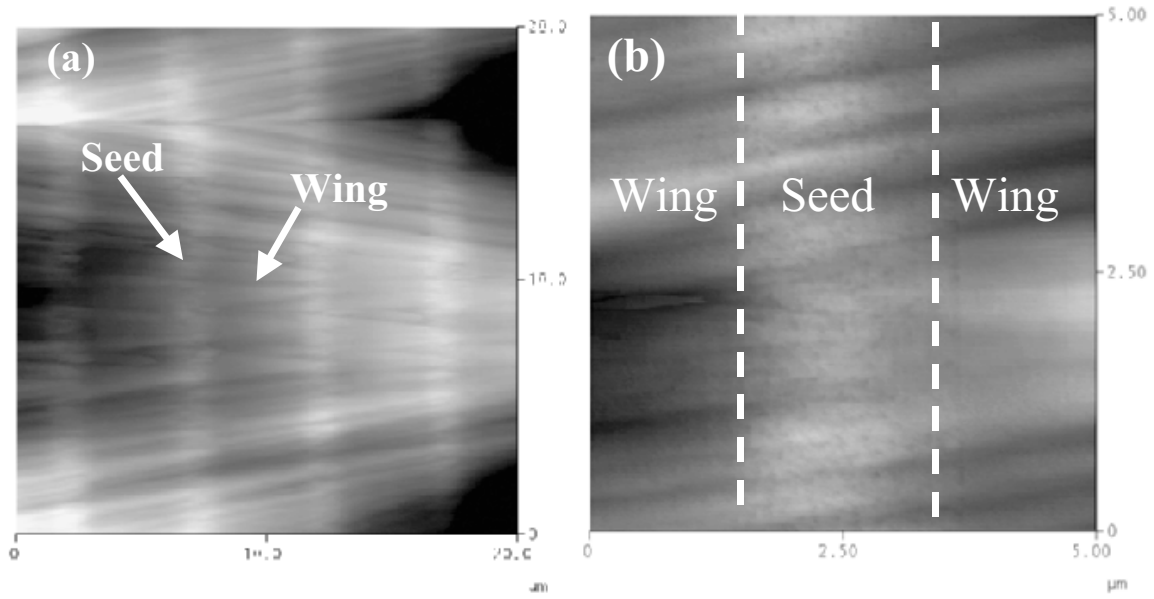

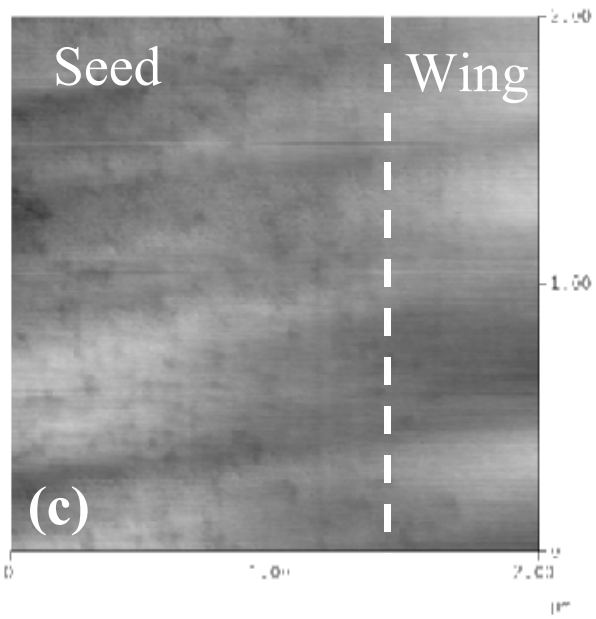

Figure 9: AFM micrographs of the surface of the coalesced pendeo-epitaxial GaN films grown at T = 1020ºC and V/III= 660. (a) 20µm x 20µm scan showing both the seed and the wing regions. (b) and (c) 5.0µm x 5.0µm and 2.0µm x 2.0µm scans, respectively, that show the differences in surface microstructure between the GaN grown on the etched stripes (seed) and the laterally grown GaN (wing).

4. Future Work

The research presented previously in chapters 2 and 3 illustrate the infant stages of non-polar GaN$(11\bar{2}0)$ on AlN/4H-SiC$(11\bar{2}0)$ substrates growth. For non-polar GaN$(11\bar{2}0)$ to become a viable material for short-wavelength photonic and high-frequency devices and applications, advances need to be made in several areas.

As presented in Appendix I, Si-doping in non-polar GaN$(11\bar{2}0)$ films displayed a dissimilar behavior to its GaN(0001) counterpart. As a result, p-type and n-type doping needs to be explored in-depth to allow basic p-n junctions to be fabricated and studied. Further, contacts and contact materials would also need to be explored to facilitate any device structures that would need to be fabricated on the GaN$(11\bar{2}0)$ films.

Defect density reduction in non-polar Pendeo-epitaxial GaN$(11\bar{2}0)$ on AlN/4H-SiC$(11\bar{2}0)$ substrates showed much promise as outlined and detailed in chapter 3. However, further studies need to be performed to mature Pendeo-epitaxial growth of GaN$(11\bar{2}0)$. The coalescence and growth process of the GaN$(11\bar{2}0)$ should be optimized beyond what was presented in chapter 3. Further studies into the effects of temperature and V/III ratio on growth rates and microstructures/morphologies needs to be done as to improve the overall quality of the coalesced films. More process variables should be included in the process optimization including, but not exclusive to, growth pressure, and changing the V/III

ratio by manipulating the TMG/H_2 carrier instead of the ammonia flow. In addition, alternate stripe orientations to $[1\bar{1}00]$ should be explored, namely [0001].

Appendices

4. Appendix I: Chapter 2 Addendum

4.1 Experimental Procedure

Secondary Ion Mass Spectrometry (SIMS) analyses of oxygen, hydrogen, carbon, and silicon in GaN(0001) and GaN $(11\bar{2}0)$ thin films were conducted using a CAMECA IMS-6F, a Cs^+ primary ion beam with an energy and current of 5.5keV and 70nA, respectively, and a 200μm x 200μm rastered area. The negative secondary ions were detected from a 60μm diameter region at the center of the crater produced by the primary beam. Concentrations of the elements of interest were established by similar analyses of GaN films implanted with the elements of interest.

Photoluminescence (PL) spectra were acquired at 1.8K from a loosely focused spot using the 335.8 nm line of an 8mW Ar^+ laser. All spectra were corrected for the spectral response of the measurement system.

Capacitance-Voltage (CV) measurements of N_D-N_A were conducted on undoped and doped GaN films using a mercury probe station in tandem with a Hewlett-Packard network analyzer having a 1kHz-1MHz frequency range. The diameters of the large area ohmic contact probe and the small area Schottky contact probe were 760μm and 15μm, respectively; the distance between the two probes was 15μm. For the Hall measurements, Ti (200A) / Al (200A) contacts were deposited using electron beam evaporation, and subsequently annealed in forming gas at 750^{o}C for 45 seconds.

4.2 Results and Discussion

Donor doping of [0001]- and $[000\bar{1}]$-oriented GaN epitaxial thin films with Si was achieved via incorporation of SiH_4 (silane) into the reactant gas flow. Process optimization of the MOVPE system described in Section 2.3 allowed the establishment of growth parameters that resulted in expected values of N_D-N_A. The chart used to determine the SiH_4 flow rate (μmol/min) needed to achieve the desired carrier concentration is shown in Figure 1. It should be noted that the measured carrier concentrations for each of the data points used in figure 1 were determined using Hall measurements. Using the equation given in figure 1, carrier concentrations of 3E+17, 1E+18, and 1E19 for c-plane GaN (0001) were selected and the corresponding flow rates of SiH_4 were determined. Six samples were produced over 3 growth runs where there was one 4H-SiC $(11\bar{2}0)$ piece and one 6H-SiC(0001) piece per growth run. This was to ensure that the samples being used in comparison were produced under the exact same conditions. The undoped a-plane and c-plane GaN samples discussed in the succeeding text were not produced during the same growth run, but the same growth parameters were used.

Table 1 shows the results of depth profile C-V measurements performed at 1MHz. The depth profiles were constant for all samples. The expected ND-NA values for the c-plane samples are also stated for a point of reference, along with the SiH4 flow rates (μmol/min) used for n-type carrier doping.

Examination of the C-V data shows that the behavior of the a-plane GaN $(11\bar{2}0)$ samples is different from that of the c-plane GaN(0001) samples despite the fact that the amount of molar flow rates of SiH4 for each of the comparison

growth runs were equivalent. As a result, SIMS analysis was performed to (1) determine the amount of atomic Si incorporated into concurrently produced a-plane and c-plane GaN, and (2) to determine the atomic concentrations of H,C, and O species for Si doped and undoped GaN samples.

Figure 2 shows the SIMS results for the Si doped GaN. The expected Si concentration (atoms/cm3) for these samples was 3E+18. SIMS shows that the atomic % Si in the a-plane and c-plane samples were 3E+18 and 2E+18, respectively. This indicates that there is, in fact, practically equivalent amounts of the n-type carrier, Si, in each of the films, and that unequal concentrations of Si in the GaN films, regardless of the plane in question, does not explain the dissimilar behaviors shown in the depth profile C-V analysis performed at 1MHz. Figure 3 shows the SIMS results for the Si doped a-plane and c-plane GaN samples investigating the concentrations of the H, C, and O species. The SIMS shows that the Si doped GaN $(11\bar{2}0)$ samples have more H, C, and O contamination than the GaN(0001) samples. The c-plane GaN(0001) H, C, and O concentrations are very close to the detection limit. Figure 4 shows the SIMS results for the undoped a-plane and c-plane GaN samples investigating the concentrations of the H, C, and O species. The SIMS shows that the contamination of the H species in the GaN $(11\bar{2}0)$ sample is higher than in the GaN(0001) sample, and the C and O contamination levels are close or less than the detection limit in both samples. With SIMS analysis showing no clear differences in Si concentrations or impurity concentration in the films, no conclusions for the divergent C-V behavior in the GaN(0001) and GaN $(11\bar{2}0)$ films could be proposed.

Photlouminescence was performed to compare the effects of Si-doping on GaN $(11\bar{2}0)$ and GaN(0001) films, while using undoped GaN $(11\bar{2}0)$ and GaN(0001) films as a point of comparison. Figure 5 shows the PL spectra for doped and undoped GaN(0001). The bottom spectrum is for undoped GaN(0001). The spectrum shows a strong, reasonably sharp (5.5 meV FWHM) neutral donor-bound exciton (D^o, X) peak at 3.4852 eV with a LO phonon replica at 3.3922eV. The top spectrum is Si-doped GaN(0001). The spectrum shows a strong, reasonably sharp (5.9 meV FWHM) (D^o, X) peak at 3.4832 eV with a LO phonon replica at 3.3916 eV. These two (D^o, X) peak positions imply substantial compressive biaxial stress. Broad yellow luminescence peaks centered at 2.2 eV are also observed for both cases. For Si-doped case, a donor-acceptor pair (D^o-A^o) peak at 3.2836 eV is observed with phonon replicas at 3.192 eV and 3.1 eV. Compared with the undoped case, it could be concluded that this donor-acceptor pair peak is related to the incorporated Si.

Figure 6 shows the spectra of doped and undoped GaN $(11\bar{2}0)$. The bottom spectrum is from undoped GaN $(11\bar{2}0)$. A broad PL band is observed at 3.258 eV with higher energy shoulders at 3.337 eV and 3.392 eV. This band is probably associated with stacking faults (SF) in the material. The top spectrum is from Si-doped GaN $(11\bar{2}0)$. A broad PL band is observed at 3.292 eV with a higher energy shoulder at 3.385 eV (probably same origin as in BW-845). Broad deep level PL bands are observed around 2.1 eV for both cases. The apparent downshift in the yellow band peak position may imply that it originates primarily from the faulted (cubic) regions. Normal wurtzite GaN exciton peaks, which are located between 3.45 eV and 3.5 eV are not observed. Figure 7 shows PL spectra of undoped GaN(0001) and GaN $(11\bar{2}0)$.

Figure 8 shows PL spectra for Si-doped GaN(0001) and GaN$(11\bar{2}0)$. The spectra presented in Figures 7 and 8 are the same spectra from Figures 5 and 6. No new conclusions can be made from Figures 7 and 8 but they help to illustrate the observations discussed previously.

The above PL spectra comparisons show no distinct differences that could support a reasonable hypothesis for the seemingly irreconcilable behavior of the GaN(0001) and GaN$(11\bar{2}0)$ films characterized by C-V measurements. However, the SIMS and PL data for the GaN discussed previously add to the overall understanding of GaN$(11\bar{2}0)$ films on 4H-SiC$(11\bar{2}0)$ substrates.

4.3 Tables

Table 1: Depth profile C-V results acquired at 1MHz on $[11\bar{2}0]$- and [0001]-oriented GaN thin films. Expected N_D-N_A values for GaN[0001] samples are included for reference.

GaN[0001]	GaN$[11\bar{2}0]$	SiH_4 (um/min)	Expected N_D-N_A values GaN[0001]
8.50E+17	n/a	60.16	3.00E+17
3.00E+18	3.00E+17	159.56	1.00E+18
2.00E+19	2.00E+19	1202.2	1.00E+19

4.4 Figures

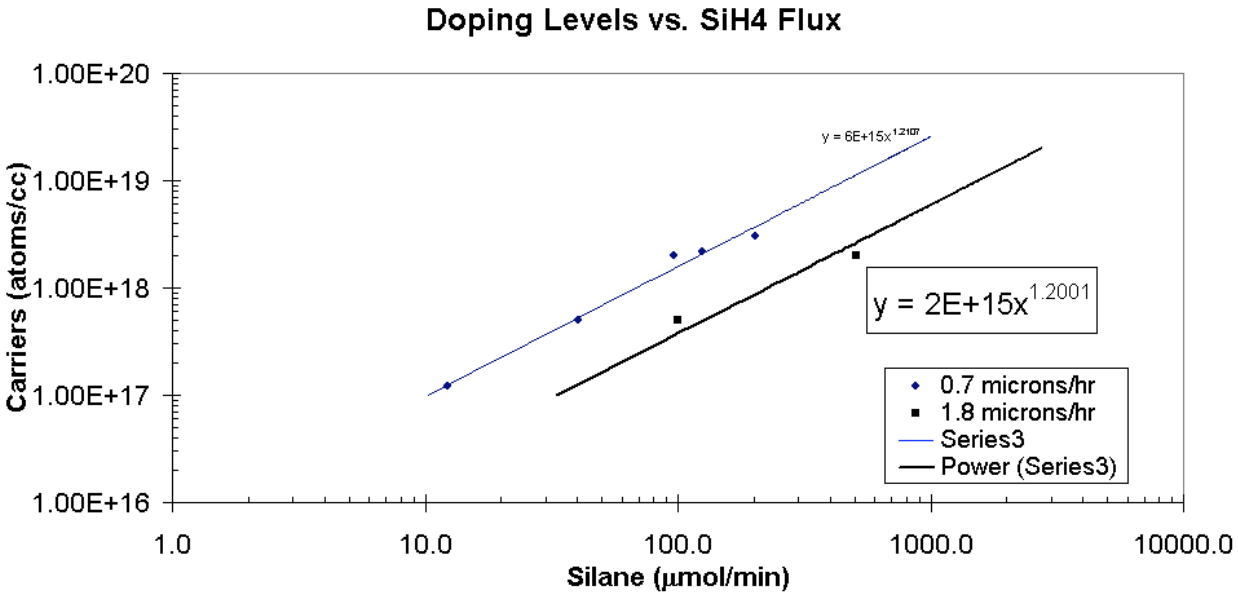

Figure 1: Graph used to predict Silane flow (µmol/min) needed to achieve the desired number of carriers in GaN(0001) thin films. As used in this instance, 1.8µm/hr is the appropriate series for prediction where the proper equation is indicated by the black box.

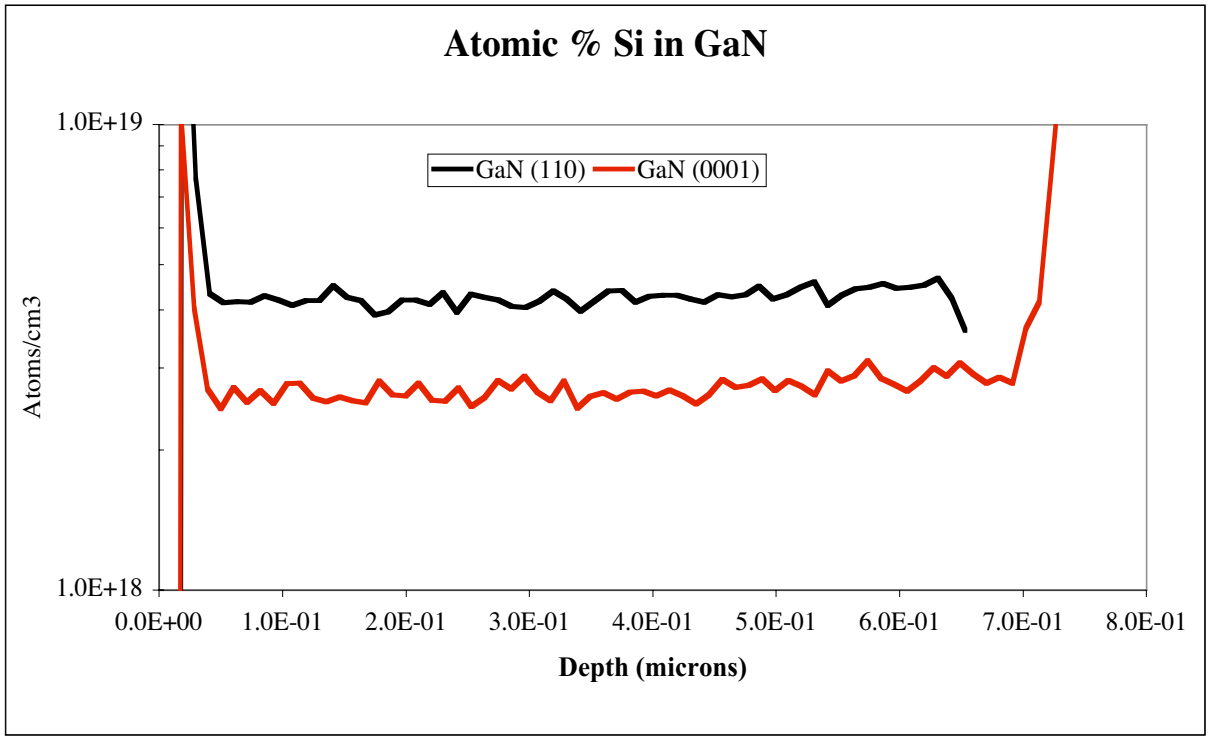

Figure 2: Atomic % Si incorporated during growth into [$11\bar{2}0$]- and [0001]-oriented GaN thin films.

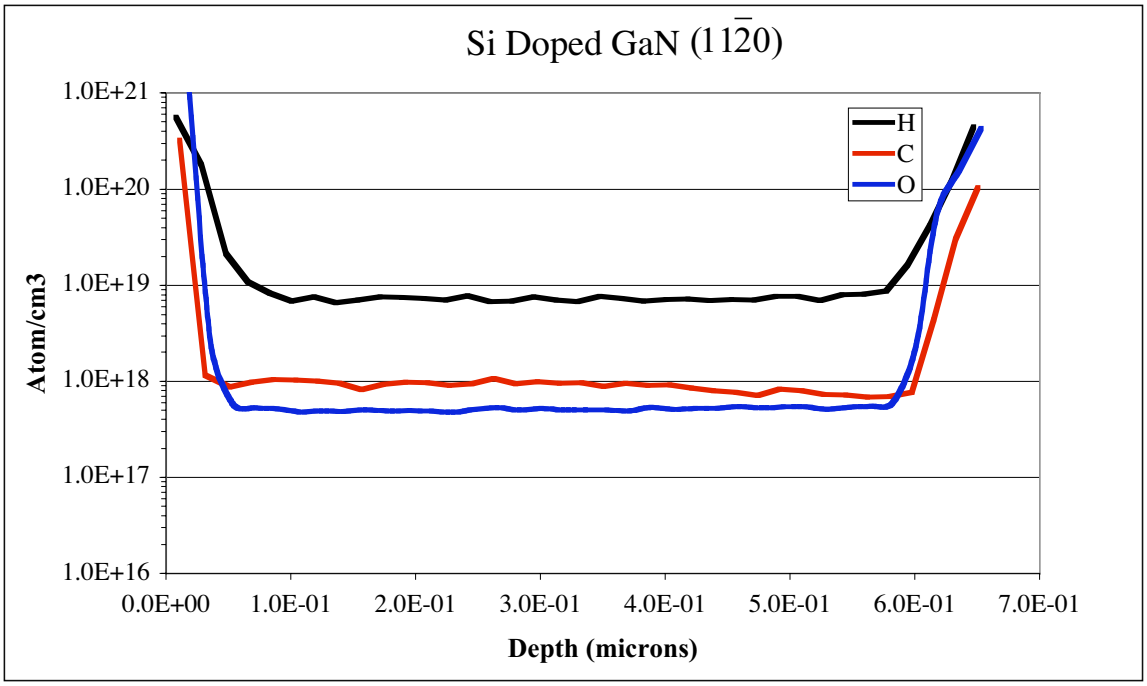

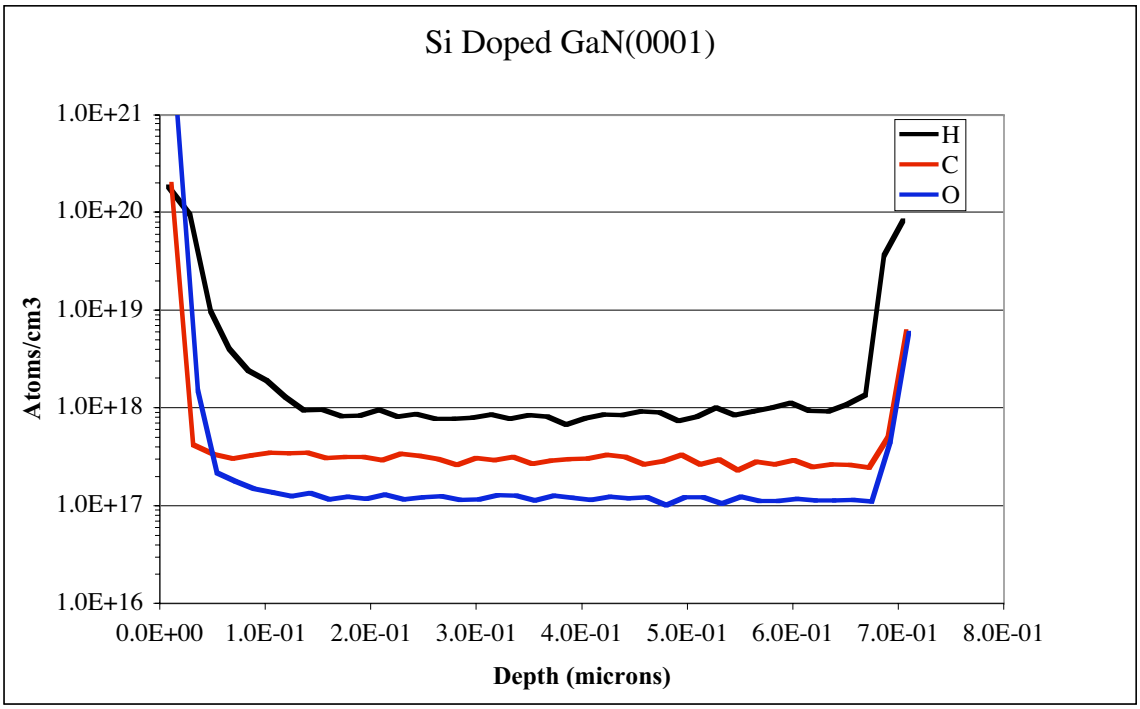

Figure 3: SIMS results of atomic concentrations of H, C, and O as a function of depth in Si-doped [11$\bar{2}$0]-and [0001]-oriented GaN thin films.

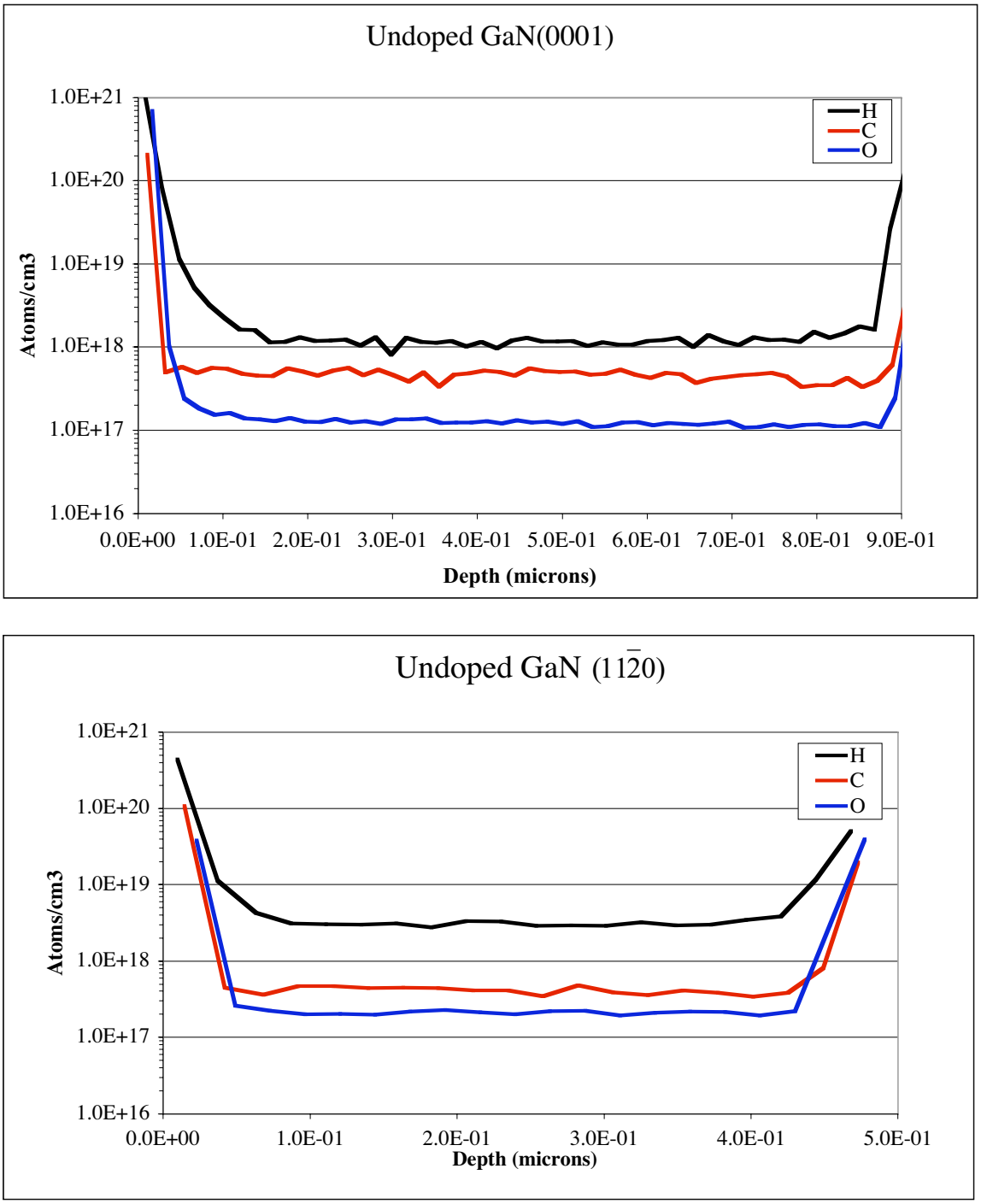

Figure 4: SIMS results of atomic concentrations of H, C, and O as a function of depth in undoped [11$\bar{2}$0]-and [0001]-oriented GaN thin films.

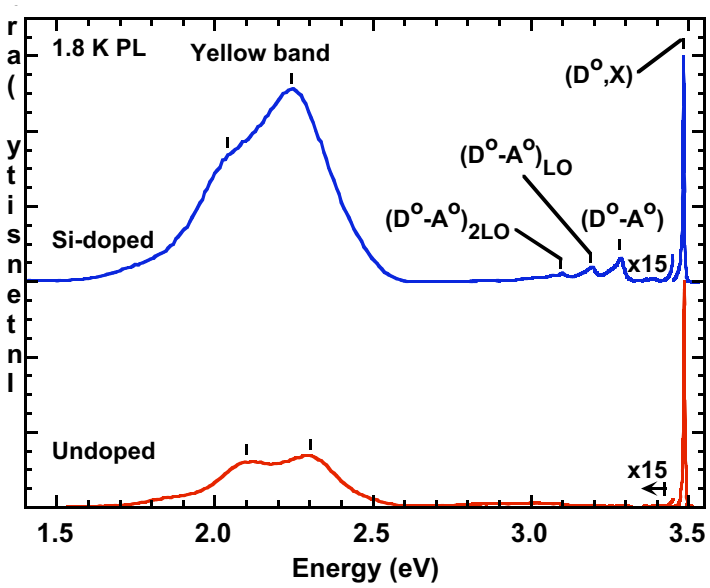

Figure 5: PL spectra of undoped and doped GaN(0001)

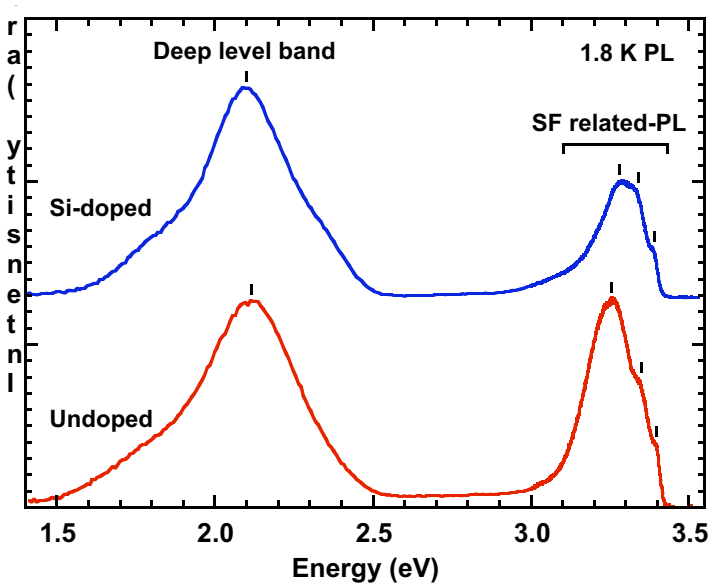

Figure 6: PL spectra of undoped and doped GaN $(11\bar{2}0)$

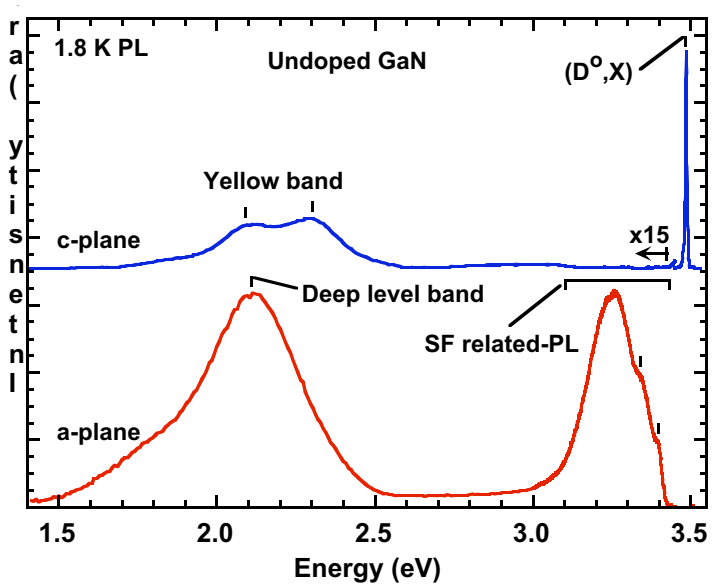

Figure 7: PL spectra of undoped GaN $(11\bar{2}0)$ and GaN(0001)

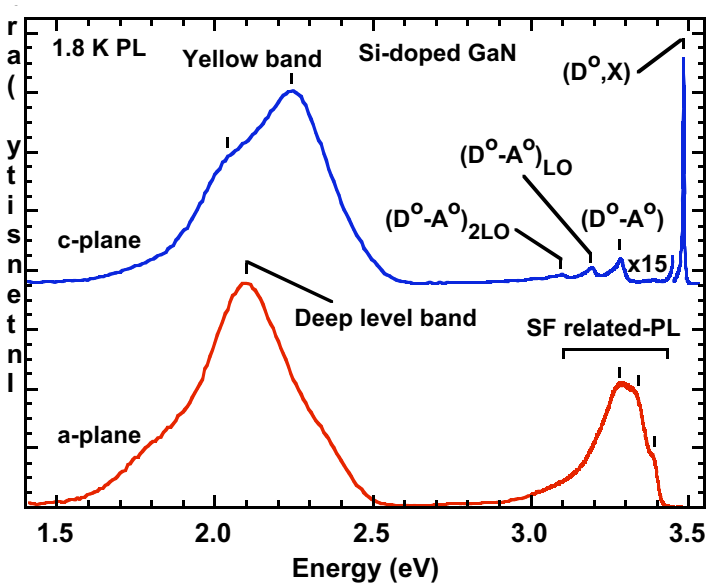

Figure 8: PL spectra of Si-doped GaN $(11\bar{2}0)$ and GaN(0001)

6. Appendix II: Pendeo-epitaxy Cleanroom Processing

6.1 Cleaning the GaN Wafers

- Using the appropriately marked beakers, clean in acetone for 5 minutes and blow dry with N_2.
- Using the appropriately marked beakers, clean in methanol for 5 minutes and blow dry with N_2.
- Bake the GaN wafers at 115°C and cool on the aluminum plate.

6.2 AZ5214E Photoresist Coating

- A Karl Suss RC-8 Photoresist Spinner is used to spin-coat the GaN wafers with AZ5214E photoresist. Corporate information on the Karl Suss RC-8 photoresist spinner, and the AZ 5214E photoresist is included in section 7.7.
- Make sure the 2 inch wafer holder is set at 4000 rpm for 40 seconds. Place the GaN wafer on the center of the wafer holder, and perform a test spin to make sure the wafer is centered on the holder. This should be done before any Photoresist (PR) is placed on the wafer.
- Using an approved eye-dropper, put a quarter-sized amount of PR in the center of the GaN wafer and spin coat at the settings mentioned in the previous step.
- Soft-bake for 2 minutes at 90°C and cool on the aluminum plate.

6.3 Alignment and Exposure

- Clean the desired mask by spraying the metal side of the mask with mask cleaner. Rinse both sides with water and blow dry with N_2.
- A Karl Suss MJB-3 aligner was used for the exposure of the PR using a 3-3 mask. The mask results in 3 micron stripes of alternating positive and negative PR. Information on the Karl Suss MJB-3 aligner is included in section 7.7.
- Slide the wafer holder out and put in the 2 inch wafer chuck.
- Remove the mask holder, flip over, and place the mask on the holder with the metal side up.
- Turn on the power and the mask vacuum if the mask holder has a vacuum chuck.
- Load the wafer on the wafer holder making sure that the stripes in the mask are parallel to the major flat on the a-plane 4H-SiC (11.0) wafer. This ensures that the stripes are in the [1-1.0] direction.
- The large handle on the left moves the microscope, while the wafer stays stationary.
- To move the wafer while not in contact mode, use the knobs on the front and the right of the stage.

- Align the mask stripes by moving and rotating the wafer under the microscope so the stripes are parallel to the major flat, as described above.
- Use the two levers on the left side to move the wafer into contact mode with the mask. The levers should be engaged until the contact light indicates that sufficient contact between the wafer and the mask has been achieved.
- Set the exposure time to 8 seconds, double checking the units on the center of the dial. This is a common error that results in having to remove the PR from the wafer and re-starting the clean-room processing.
- Press the expose button while using a small resistive force on the microscope with your hand. This prevents the exposure source and microscope from moving forward too abruptly and disrupting the proper alignment of the mask with the primary flat of the GaN wafer.
- Bake the exposed PR coated wafer at 115°C for 1.5 minutes
- Using the MJB-3 aligner, remove the mask and do a flood exposure for 1.5 minutes. Double check the units on the exposure timer, as this is a common error.

6.4 Develop

- Develop the wafer in MF-319 developer. Usage of a separate beaker for the developer and wafer basket is recommended over using a developing bath.
- After desired develop time, rinse in DI water bath.
- Check the pattern development under an optical microscope to determine if the developing is complete or if more developing is needed.
- Suggested develop time for use of AZ5214E PR in combination with the steps listed previously is ~150 seconds. This develop time may need to be adjusted if any of the process parameters or steps must be altered for any reason. If time adjustment is needed, then it is suggested that the development be done in several developing steps as to avoid over-developing the PR.

6.5 Nickel Deposition

- First, clean the PR patterned GaN wafers for 5 minutes in room temperature HCl using a 1:1 DI water to acid ratio. Blow dry with N_2.
- Bring the E-beam deposition system to atmospheric pressure by opening the vent valve and raise the bell jar.
- Load the GaN wafers, the crucible and Ni in the boat and a crystal in the quartz crystal monitor. Make sure the chimney above the Ni crucible is centered. Also make sure that the filament is below the Ni boat.
- Lower the bell jar and rough out the system by closing the backing valve and opening the roughing valve.
- Pump down to 0.2 torr and then close the roughing pump valve, open the backing pump valve and then open the diffusion pump valve.
- Pump down to 5E-6 torr. Turn on the ion gauge to read pressure.

- Fill the cold trap with liquid N_2. Open the liquid N_2 valve until a large white cloud forms on the ceiling. Filling once during the pump down also helps with the pump down time
- Turn on the water interlock switch, turn on the high-voltage to the e-beam and turn on the filament current.
- Turn on the quartz crystal monitor and enter the correct z-factor and density for the metal being deposited (found in the system log book)
- Slowly ramp up the filament current at a rate of 0.2 A per 30 seconds. Around 3.0A deposition should occur.
- Once deposition rate reaches 0.3 A/s, slowly open the shutter and hold in place with a set screw.
- Deposit the first 50A of Ni at a slow rate of 0.3A/s
- Deposit the next 100A at a rate of 0.5A/s. Ramping up the deposition rate is accomplished by increasing the filament current.
- Slowly increase the deposition rate to 2.0A/s until 1500A has been deposited. If the GaN wafers are thicker than 1um, a thicker Ni layer should be deposited.
- Once a thickness of 1500A has been reached, SLOWLY close the shutter.
- Continuously turn down the filament current, turn off the filament and turn off the high-voltage.
- Allow the system ten minutes to cool down.
- Turn off the ion gauge and shut the valve to the diffusion pump (HI-VAC).
- Bring the system up to atmosphere by switching on the vent valve and raise the bell jar.
- Unload the samples, the quartz crystal and the Ni crucible. Due to the heating nature of Ni, the crucible will be cracked and can be used one or two more times.
- Lower the bell jar and return the system to stand-by mode by pumping with the roughing pump down to 20 mtorr.
- Turn off the water interlock and fill out the log book.

6.6 Lift-off

- Place Ni deposited wafers in a clean beaker with acetone for 1 hour.
- After 1 hour, place the beaker with the wafer still in the acetone in a sonic bath for 15 seconds.
- If lift-off is incomplete, use a swab and carefully wipe along the stripe direction.
- Blow-dry wafer with N_2.
- Check for satisfactory lift-off under an optical microscope.
- After lift-off is complete, the wafer is ready for ICP etching.
- After ICP etching, remove the Ni stripes by placing the etched GaN template in a 1:1 HNO_3 acid to DI water solution for 8 minutes.
- Blow-dry with N_2.

6.7 Pendeo-epitaxy Cleanroom Process Chemical Details

- AZ5214E Photoresist
  Hoechst Celanese Co.
  Electronic Products Division, AZ photoresist products
  170 Meister Ave. Somerville, NJ 08876 USA

- Microposit MF-319 Developer
  Shipley Company
  455 Forest St.
  Marlborough, MA 01752

- Karl Suss RC-8 PR Spinner and MJB-3 Aligner
  SUSS MicroTec Inc.
  228 SUSS Drive
  Waterbury Center, VT
  05677-0157 USA